Basin Research (1999) **11,** 21–41

Development of mountainous topography in the Basin Ranges, USA

M. A. Ellis,* A. L. Densmore† and R. S. Anderson‡

**Center for Earthquake Research and Information, University of Memphis, Memphis TN 38125, USA*
†Department of Geology, Trinity College, Dublin 2 Ireland
‡Institute of Tectonics and Department of Earth Sciences, University of California, Santa Cruz, CA 95064, USA

'The Basin ranges…offer unusually simple examples of mountain uplift and sculpture; examples that may be adduced as relatively elementary illustrations of the difficult group of mountains in general, and that may therefore be with propriety presented to beginners for introductory practice before the description of complicated mountain ranges is undertaken.'

W. M. Davis, 1903, p. 130.

ABSTRACT

We use the landcape evolution model *Zscape* to explore quantitatively the development of mountainous topography in the Basin and Range province (formerly the Basin Ranges), USA, as a function of faulting, surface processes and microclimate. Many of the classic morphologies of mountains in the Basin and Range were described in the late part of the 19th century. The varied topography coupled with di ering experiences led to a similarly diverse set of explanations. We are able to demonstrate through a variety of numerical experiments that a diverse landscape is easily obtained by the simple, steady combination of tectonic and surface processes. Numerical landscapes reveal the same features observed in the field, including facets, spur benches, piedmonts, and relatively linear and regularly spaced drainages. In all cases, a steady-state landscape is generated on the order of 10^6 years, so that there remains little information in the landscape that can tell us about processes or conditions prior to 1 million years ago. The fundamental form of the steady-state landscape (including the facet and spur bench morphology) is governed by the spacing of rivers and bedrock strength and the resulting relief is for the most part strength-limited. Neither hillslope nor facet relief is dependent on the rate of fault slip or channel incision. Relief is incision-limited, however, nearer the headwaters of rivers where stream power is relatively low. Topographically asymmetric ranges may be generated over tectonically symmetric horsts by allowing precipitation to be driven by orographic processes, but the asymmetry is likely to be dependent on the ability to remove eroded material from the adjacent basins. The value of the experiments presented here is to demonstrate that the astute and impressive observations made by the likes of Gilbert, Davis and Dutton are reproducible using a relatively simple description of the relevant physics and that we can recognize and explain various landscape morphologies that have in the past been the subject of necessarily qualtitative reasoning.

INTRODUCTION

Regional topography of the western United States (Fig. 1) has been used extensively in the development of tectonic models for the origin of the Basin and Range province (e.g. Stewart, 1978; Eaton, 1982; Sonder *et al.*, 1987; Wernicke, 1992; Harry *et al.*, 1993; Byrd *et al.*, 1994). Less attention has been paid to the topography of individual mountain ranges, particularly within the context of a coupled tectonic–geomorphic system. Mountainous topography in the Basin and Range is generally considered superficial to the structural or

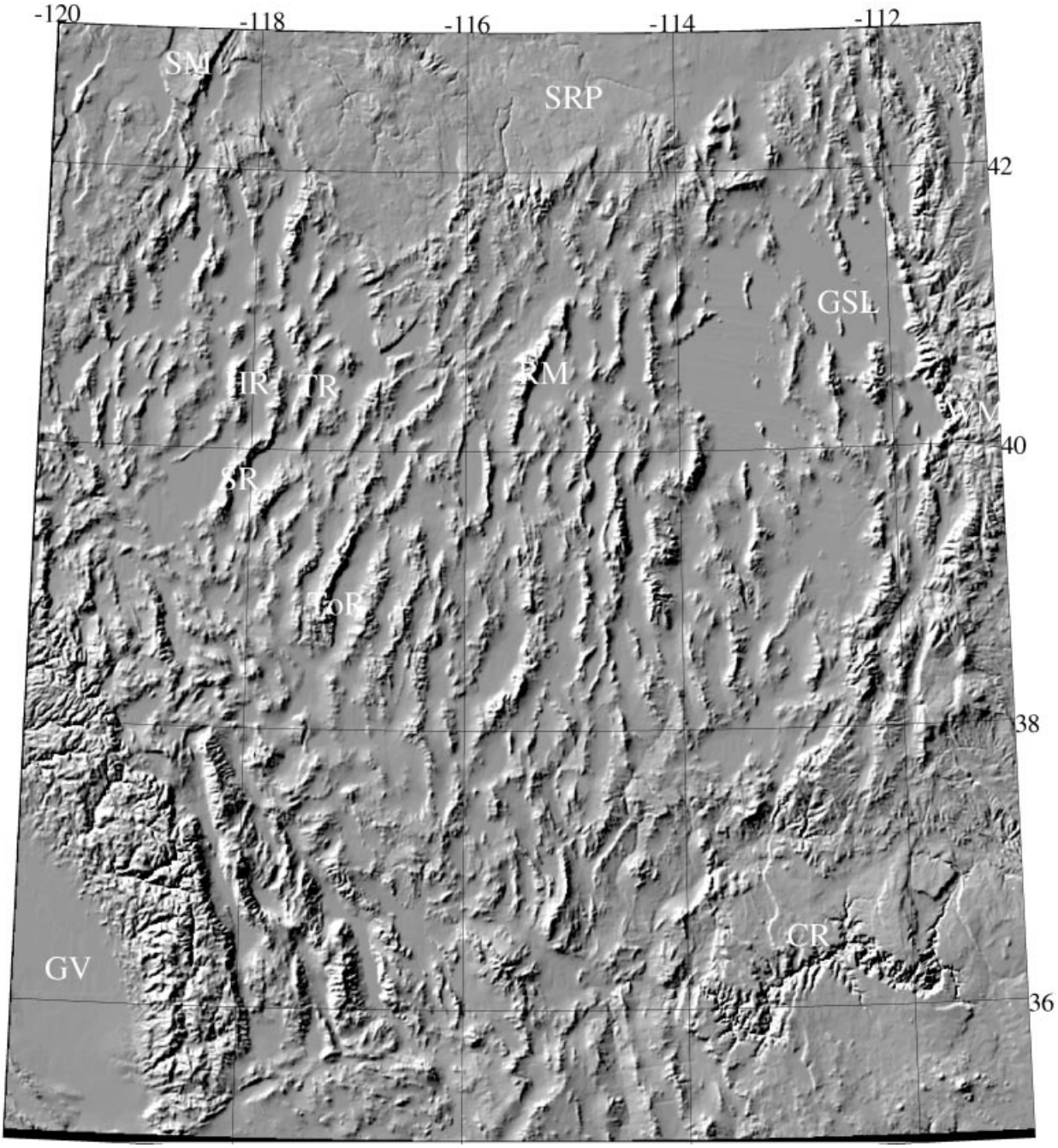

Fig. 1. Shaded-relief image of the Basin and Range, derived from USGS 30 arcsec Digital Chart of the World DEM data. Abbreviations are as follows: CR – Colorado River; SM – Steens Mountain; SR – Stillwater Range; SRP – Snake River Plain; TR – Tobin Range; ToR – Toiyabe Range; WM – Wasatch Mountains; GSL – Great Salt Lake; HR – Humboldt Range; GV – Great Valley; RM – Ruby Mountains.

tectonic origin of the range, despite the fact that the tectonic setting provides the basic template on which surface processes act. Hidden in the morphology of these dramatic ranges is information about both the tectonic and climatic conditions that have shaped them. The extent to which such information is recoverable has in the past been limited to qualitative and unsubstantiated debate, albeit much of it with prescient insight. In this paper we explore the relations between tectonic and surface processes (which may proxy as climate) using the quantitative, process-based landscape evolution model *Zscape* (Densmore *et al.*, 1998).

In particular, we demonstrate quantitatively that the morphologies of individual mountain ranges in the Basin and Range are a sensitive measure of the interplay between tectonic and surface processes. In the following sections, we provide first a perspective on the ideas that have shaped our view of the Basin Ranges, and we summarise the essential characteristics of topography in the region. We then examine the development of

mountainous topography through a set of numerical experiments, with the goals of (1) identifying the controls on the development of typical Basin and Range landforms, (2) exploring the role of initial conditions in determining range topography and (3) examining the e ects of spatial and temporal variations in both tectonic and microclimatic patterns. We demonstrate reasonable scenarios for the origin of commonly observed range-front features, including triangular facets, spur benches and alluvial piedmonts. In ranges where uplift is accommodated by multiple faults, we illustrate the significant influence of spatial asymmetry in the tectonic and microclimatic processes.

A SCINTILLA OF HISTORY

The meaning of topography in the Basin and Range Province

At the turn of the 20th century the origin of mountains in the Basin Ranges (it was not until 1928 that the region was o cially named the Basin and Range Province (Fenneman, 1928) (Fig. 1) had two apparently diverse explanations. One suggested that the mountains were 'the net results of compound erosion active since the Jurassic times' (Spurr, 1901, p. 265), primarily due to 'vigorous di erential deflation on a region that had been previously flexed and profoundly faulted and then planed o ' (Keyes, 1910, p. 549). The second related the ranges to uplifted fault blocks of previously folded and eroded rocks, such that 'a range consisting of a faulted block generally has a bold front on the side of a fault and is less abrupt on the opposite slope. On the side of the bold front the line separating the rock of the mountain from the alluvium of the valley is simple and direct, while on the opposite side it is tortuous' (Gilbert, 1890, p. 340–341). The former, passive view was developed in part by the role model provided then by the folded and remnantal nature of the Appalachian mountains and the mesas of the Colorado Plateau. The dominance of the Appalachian model of mountain-building in American geological thought provoked Gilbert as early as 1874 to state that 'it is impossible to formulate these (ranges) by the aid of any hypothetical denudation in such a system of undulations and refoldings as the Messrs Rogers have so thoroughly demonstrated in Pennsylvania and Virginia, but the structure of the Western Cordillera system stands in strong contrast to that of the Appalachians. In the latter, corrugation has been produced commonly by folding, exceptionally by faulting; in the former commonly by faulting, exceptionally by flexure' (Gilbert, 1874, p. 50).

Beyond the expectations and experience of these investigators, the dichotomy of opinions reflects the varied topography in the Basin and Range province. Some ranges show clear evidence of the asymmetry and associated faulting described by Dutton and Gilbert (e.g. the Stillwater Range, Ruby Mountains, Wasatch Mountains, Cortez Range, Steens Mountain, Toiyabe Range, etc.), while others reveal far less (e.g. East Humboldt Range, Battle Mountain, Grapevine Mountains, Spring Mountains). Proponents of the remnantal origin cited as evidence of wind erosion the commonly observed bare rock or thinly mantled surfaces that skirt the ranges 'as to suggest at once the presence of fault scarps as an explanation of the steep faces of the mountains' (Keyes, 1909, p. 753). In other words, the sharply eroded edge of the range was being mistaken quite naturally as evidence of faulting. Added to this was the observation that faults were often 'far out in the plain, often at a distance of 4 or 5 miles' (Keyes, 1909), and that 'although the mountain may be a faulted block…the movement is commonly discovered to be of an ancient date' (Keyes, 1909, p. 753).

The last observation is an important one, for it raises both the stumbling block as well as the common ground on which to find an answer. A principal di culty in understanding the origin of these ranges must surely have come from the unknown age of faulting and of the rates at which erosion razes the landscape and tectonics rebuilds it. Also, the recognition of fault scarps as crustal-scale faults was still in its infancy. The eyes of these investigators were tuned to faults that visibly o set stratigraphy, and small scarps running along mountain fronts frankly did not cut it. The answer lies in the astute observations of each of these past investigators and, as we describe later, is related to the interaction of tectonic and surface processes that generates what appears to be a diverse topography but that in fact contains many of the same morphological elements.

The notion that the Basin Ranges were produced by di erential fluvial erosion (Spurr, 1901) inspired the pre-eminent geographer of the times, W. M. Davis, to enter the debate (Davis, 1903). By 1903, Davis had established a set of criteria to distinguish faulted mountain fronts, and described a scenario of range front evolution that depended on the activity of the frontal fault (Davis, 1903). This scenario, closely but not wholly echoed by Gilbert (1928), is consistent with a number of topographic observations, and forms the basis for several recent interpretations of range front morphology (e.g. Hamblin, 1976; Wallace, 1978). After Gilbert's death in 1918, interest in the geological meaning of topography in the Basin and Range waned, with a few very notable exceptions (Sharp, 1940; Hamblin, 1976; Wallace, 1978; Menges, 1990; Harbor, 1997), possibly as the geological and geomorphological communities began to separate and as the ability to probe deeper into the crust improved (Merritts & Ellis, 1994). It is probably fair to suggest that most of what we currently know about range front morphology we knew shortly after the turn of the century.

Structural development of ranges

In contrast to the relative dearth of interest in the topography of the Basin and Range, ideas on its structural

history have been plentiful and in some quarters remain hotly debated. Gilbert (1874, 1928) and Dutton (1880) described fault scarps, fault-related flexure of footwall and hangingwall units, and the asymmetrical shape of many ranges that are today the stock-in-trade in Basin and Range tectonics. Interestingly, none of these studies linked these features to an extending crust. In a work completed a decade or more before its publication, Gilbert (1928) drew cross-sections with normal faults that steepen with depth, and he called on di erential vertical forces to explain the fault blocks and variable uplift patterns. Consensus at the turn of the century tied the origin of the ranges more convincingly to faulting than to erosion and, by 1925, Davis had explicitly connected the faults to the concept of crustal extension. Today, there is little doubt that the Basin and Range is an extended crustal section and that extension continues to be active at a rate of 10^{-8} to 10^{-7} yr^{-1} (Eddington *et al.*, 1987; Dixon *et al.*, 1995).

More recently, the point of contention has been on the other foot, since the existence of footwall uplift (and hence of the mountain range) was until the late 1980s considered a relative uplift only. That is, while extension of the Basin and Range had become axiomatic, ranges were pictured as remnants about which everything else (the basins) were falling (e.g. Stewart, 1978). A number of studies over the past two decades, however, show that rock uplift of footwalls is commonly very high (up to $\approx$10 km) and localized (King & Ellis, 1990). Footwall uplift involves both rock and surface uplift, relative to a regional level, which itself was likely to be subsiding (Wolfe *et al.*, 1997). There are, undoubtedly, some di erences in the details of the various proposed mechanisms of footwall uplift (Buck, 1988; Hamilton, 1988, 1989; Wernicke & Axen, 1988; King & Ellis, 1990; Wernicke, 1992) but none of these models di ers in their fundamental method of delivering rocks to the surface via high-angle, normal faults. Focal mechanisms show that much of the present-day seismicity of the Basin and Range occurs on high-angle faults (e.g. Doser & Smith, 1989; Jackson & White, 1989). The role of low-angle normal faults in exhuming crustal material was significant during Palaeogene and early Neogene times, but appears today to be relatively restricted (e.g. Burchfiel *et al.*, 1987; Hodges *et al.*, 1989; Caskey *et al.*, 1998).

The fundamental tectonic uplift of a mountain in an extensional regime (Fig. 2) is caused by the restoring moment-arm of a flexed beam (Weissel & Karner, 1989). Uplift continues in response to restoring isostatic forces brought about by modifying the spatial pattern of surface loads via erosion and deposition (King *et al.*, 1988; Stein *et al.*, 1988) and may be increased and localized further still by allowing such isostatic restoring forces to help drive fault displacements (King & Ellis, 1990).

Earlier numerical experiments suggest that the pattern of mass redistribution during the evolution of basin-range systems, including the extent to which the system remains open or closed to mass loss, may profoundly a ect the magnitude and asymmetry of exhumation and

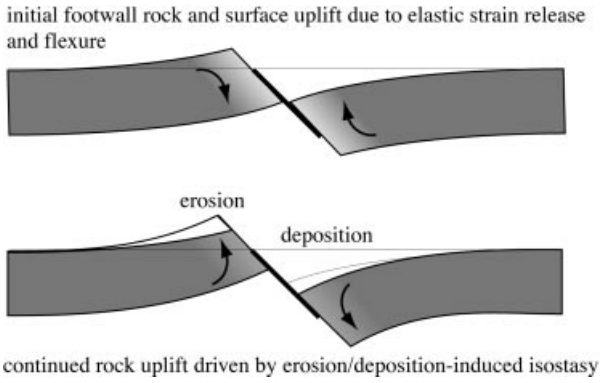

Fig. 2. Schematic illustration of the origin of ranges in the Basin and Range Province (e.g. Buck, 1988; King & Ellis, 1990). The energy to drive this deformation comes from the combination of gravity (the release of gravitational potential energy), plate boundary tractions and the flexed-beam upper crust. Arrows in the upper diagram show the restoring moment of a flexed beam, the energy for which is within so-called fibre stresses within the beam while the energy required to drive displacement across the fault is taken from the beam adjacent to the fault. Arrows in the lower diagram show the isostatic restoring forces due to unloading (erosion) and loading (sedimentation) of the footwall and hangingwall, respectively. Whether the isostatic restoring forces are used to drive further displacement of the fault (as in King & Ellis, 1990) or are distributed uniformly (as in Buck, 1988) determines the exact geometry of the range and basin deformation. In either case, erosion and sedimentation enhance and localize uplift and subsidence.

subsidence (Ellis, 1991). The length-scale of coupling between surface and crustal process may be dictated by the degree of communication between separate ranges; for example, changes in base-level e ected by one fault-bounded range will ultimately a ect the development of other ranges if they are linked by an axial drainage system (e.g. Sharp, 1940).

TOPOGRAPHY OF THE BASIN AND RANGE PROVINCE

The average elevation of the Basin and Range is $\approx$1400 m, similar to that of the interior of the Colorado Plateau. Various explanations exist for the relatively high average elevation, including doubling of the lithosphere by earlier subduction of the hot and buoyant Farallon plate (Bird, 1989), thickening of the crust during the Sevier Orogeny (Bartley & Wernicke, 1984; Sonder *et al.*, 1987) and regional uplift by isostatic compensation owing to the replacement of dense upper mantle by less dense asthenospheric material as the lithosphere is stretched (Lachenbruch & Sass, 1978; Eaton, 1982). The latter appears most consistent with the limited heat flow data (Lachenbruch & Sass, 1978) and with the distribution of gravitational potential energy (Jones *et al.*, 1996). The eastern and western boundaries of the Basin and Range are characterized by low elevations, relatively high seismic activity and heat flow, and active or at least very young

volcanism. These boundaries are well defined by significant normal fault systems that define the Wasatch Mountains in the east and the Sierra Nevada in the west. The most striking feature within the Basin and Range province, however, is the parallelism of the internal mountain ranges, which prompted Dutton (1880) to describe the map view of the province as mimicking an army of northward crawling caterpillars.

The interaction of faulting and surface processes has produced a number of distinctive morphologies in Basin and Range mountains. Many of the ranges are elongate, subparallel and with a central drainage divide running roughly along the long axis of the range. The major catchments that drain the range often trend nearly normal to this central crest, and are separated by a set of spurs (Wallace, 1978). Draped over this framework are a number of distinctive landforms, such as triangular facets, spur benches, wine-glass canyons and regularly spaced catchments (Fig. 3). Skirting the range and on the active hangingwall lies the piedmont area, whose origin is necessarily linked to that of the range itself. The piedmont may consist of a set of alluvial or debris-flow fans, possibly coalesced to form a bajada, or it may be a pediment. We describe these features and their current explanations in more detail later and in the context of our own results.

The present climate in the Basin and Range is arid, which, combined with the relatively slow rates of tectonic activity typical of the region (Wallace, 1978), implies that rates of landform generation and landscape evolution are extremely slow. Bedrock weathering rates in the region are on the order of a few to 10 μm yr^{-1} (Bierman, 1994; Small & Anderson, 1996), and hillslopes in many of the ranges are typically bare bedrock or at most thinly mantled with alluvium. Several workers have argued that much of the present topography must have been sculpted during past glacial epochs, when precipitation rates were considerably higher than present (e.g. Spaulding, 1985) and when glaciers eroded large amounts of rock from the ranges, to be deposited on the neighbouring piedmonts. Blair & McPherson (1994) have recently questioned this view of Basin and Range topographic evolution, arguing that removal of material from the footwall and alluvial fan construction is inherently episodic, and need not be dependent on climate change. Regardless of the details of this debate, an understanding of the possible evolutionary histories of these ranges, and of the landforms contained within them, requires that we observe the interactions between tectonic and climatic processes over comparatively long (i.e. several million year) time-scales. Numerical landscape evolution models are uniquely suited to this task, as they allow the exploration of topographic sensitivity to the relative roles of a variety of tectonic and climatic processes (Densmore *et al*., 1998).

Zscape: A LANDSCAPE EVOLUTION MODEL

To explore the development and significance of these distinctive landforms, we examine a set of synthetic landscapes generated by the numerical landscape evolution model (LEM), *Zscape* (Densmore *et al*., 1998). *Zscape* is a finite-di erence landscape evolution model that incorporates the three-dimensional e ects of both tectonic and surface processes (Appendix). The tectonic component of deformation is characterized by a fully three-dimensional displacement field generated (via half-space elastic modelling using 3 , Gomberg & Ellis, 1994) in response to crustal scale faulting. Each infinitesimal increment of deformation is regarded as a coseismic displacement field resulting from an earthquake, and the deformation pattern (that may vary over time) becomes the surface uplift template that is inexorably denuded by surface processes. The displacement pattern used in the current experiments is derived from a model planar normal fault of 20 km length, ≈15 km depth, and a dip of 45°. The fault is driven by a far-field uniform pure shear with a maximum extension rate of 10^{-7} yr^{-1}. This strain field (that is converted to a stress field assuming elastic isotropy) yields an average displacement on the fault of ≈1.5 m, so that the model earthquake is approximately of moment-magnitude 7. The use of a displacement field derived from an elastic model as an increment of permanent deformation may seem at first contradictory. It is important to realize that displacement across a fault is driven by deviatoric stresses and that, after the earthquake, most of the stress is already relaxed. That is, most of the displacements observed are already permanent. The elastic strains are those associated with the edge of the fault, since here the gradients of displacement are the largest. We assume that these tip-zone stresses are relaxed and strains made permanent over time through the action of various deformation mechanisms, including microfracturing (e.g. aftershocks), pressure solution, etc. This is consistent with the common occurrence of finite structures (including topography) found along the edges of faults. We use here only the central 10 km of that displacement field, so that most but not all of the displacements occur in the vertical plane perpendicular to the fault trace, which is why figures of the uplift pattern (e.g. Fig. 4) are shown on cross-sectional planes.

Surface processes are divided into several components. We simulate the conversion of bedrock to erodible regolith with a modified gamma function, in which the regolith production rate is highest beneath a thin but nonzero cover of existing regolith (Ahnert, 1970; Heimsath *et al*., 1997). Downslope regolith transport is modelled as linear, weathering-limited di usion, which serves to smooth out short-wavelength topographic roughness (e.g. Hanks *et al*., 1984; Anderson & Humphrey, 1989). For steep slopes, most of the material leaving the hillslopes does so in the form of large, bedrock landslides. In the model, these landslides are considered to be a stochastic process; the instantaneous probability of landsliding at any point is equal to the ratio of the actual hillslope height to the maximum stable hillslope height (as defined by the Culmann criterion; Schmidt & Montgomery, 1995),

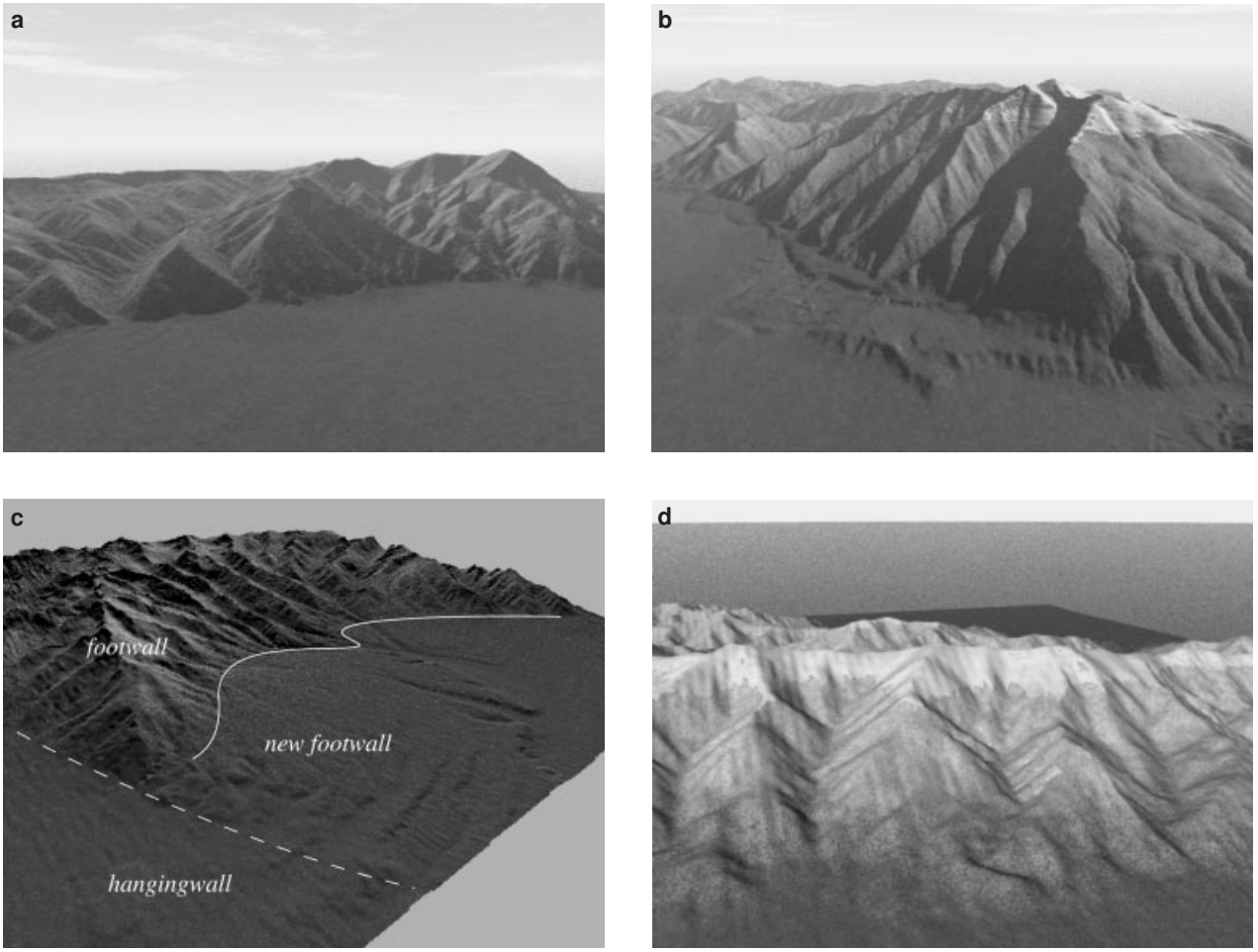

Fig. 3. Views of various ranges in the Basin and Range province, western USA. (a) Triangular facets on the north flank of the Cortez Range, north-central Nevada. An active normal fault scarp is exposed at the mountain front. (b) Triangular facets and drainages, ridgetop benches along Spanish Fork Peak, central Wasatch Range, Utah. (c) A newly forming (?) pediment on the western flank of the Ruby Mountains, near Lee Flat, north-west Nevada. The continuous white line shows the range-front that is probably occupied by an active fault whose rate of slip is lower than the range front fault in the foreground, shown by the dashed line, and which has geologically recently broken across the skirting piedmont of the hangingwall. Thus part of what used to be hangingwall is now being lifted up as part of the footwall to the younger fault, and this part of the piedmont is now in a transition between deposition and erosion. This is similar to the condition modelled in experiment 2 in which the fault is stepped out into the hangingwall (see Fig. 11). (Erosion of the piedmont is not as visible in this image as it is in the field.) (d) View of triangular facets and relatively linear and equally spaced channels on the eastern flank of the Toiyabe Range, central Nevada. (The very regularly spaced 'avalanche chutes' toward the ridge are errors in the original DEM.) Each image here was generated from a USGS 7.5 minute DEM, using Natural Scene Designer™ by Natural Graphics.

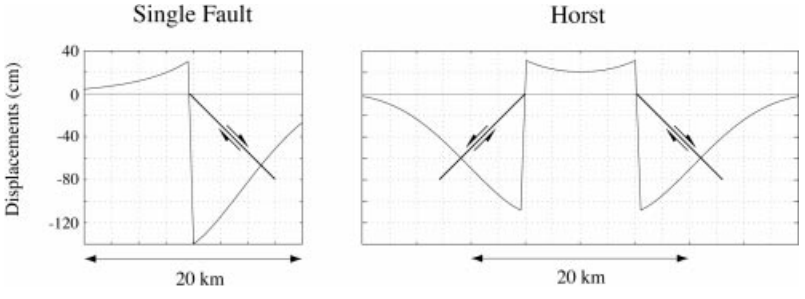

Fig. 4. Fault-perpendicular cross-sections of the displacement fields used in our experiments. Displacements vary both across and along strike. Displacement of an initially horizontal ground surface shown here is taken half way along the fault; displacement diminishes both in and out of the cross-section, toward each end of the fault. Note that horizontal scales are in km, while vertical scales are in cm. Left, single-fault displacement field used in experiments 1 and 2. Right, two-fault displacement field used in experiments 4 and 5. Each fault dips at 45°.

which is in turn a function of the landscape-averaged rock strength. Landslide debris is transported via an algorithm that distributes the failed material down the line of steepest descent, with the down-slope and cross-slope surface gradients of the debris deposits specified by the user in degrees. The experiments run here use down-slope and cross-slope of 1° and 3°, respectively. Debris is confined to a deposit three nodes wide, so that its maximum width is of the order of 300 m. This has the e ect of making our landslide debris deposits morphologically similar to typical debris flows in the Basin and Range, although we emphasize that we have not attempted here to base this algorithm on the complex physics of debris flows. Finally, a fluvial channel network is allowed to self-define on the basis of spatial variations in stream power (Bagnold, 1977), which is taken to be proportional to the product of the drainage area (a proxy for stream discharge) and local slope. Channels exist wherever this power is above a specified threshold (Montgomery & Dietrich, 1992). Fluvial sediment transport, and bedrock incision in the absence of sediment, is directly proportional to the available stream power (Hancock *et al.*, 1999). In sum, the model surface processes redistribute material on the ground surface and operate as three-dimensionally as do surface processes in the real world.

Zscape, in its current form, is the only landscape evolution model that incorporates detailed three-dimensional tectonic displacements, and that accounts explicitly for the stochastic nature of bedrock landslides. As such, the model is ideally suited to model three-dimensional variations in erosion and deposition over time-scales of 10^4–10^6 years. The natural outcome of incorporating bedrock landslides is a nonlinearity to the sediment flux rule, without the necessity of having to choose (or guess) explicitly the magnitude of the appropriate exponents. We emphasize that the process rules used in *Zscape* are physically based wherever possible, so that the results might be understood in terms of the interaction of these processes. (It would be an interesting exercise to reproduce the results obtained here with a di usion-only LEM in order to constrain the magnitude of the nonlinear parameterization in these models.) It is impossible or at least impractical to do this down to the limit of inspection (we prefer not to model atomic interactions), so that to some extent we map physical processes into so-called macrocausal descriptions (e.g. the use of stream power to initiate channels, transport bedload and incise bedrock). This means, of course, that our interpretations are limited to the scale of processes that operate at or above this level. Thus we cannot interpret our results in terms of bedload fraction or in terms of hydrological processes. *Zscape* does not currently incorporate isostatic response to the mass redistribution, and we emphasize too that there is currently no feedback between the surface processes and tectonics. The incorporation of both of the elements will be important when we begin to investigate longer-length scale features, but for the current set of experiments we do not consider these omissions to be serious (see also Densmore *et al.*, 1998).

EXPERIMENTAL RESULTS AND INTERPRETATION OF SPECIFIC LANDFORMS

We present results from a set of numerical experiments, details of which are given in respective figure captions, the Appendix, in Table 1, or in the body of the text. For the purposes of this paper, we restrict our attention to the relief generated by high-angle faults. Unless otherwise noted below, the experiments generate synthetic landscapes that are 10×10 km in spatial extent, have a grid spacing of 100 m and have typical model run times of 1000–2000 kyr. Displacements are applied in discrete 'earthquakes' every 500 years of model run time. We first

Table 1. Model parameters.

Parameter	Value	Symbol	Reference
β_{crit}	34°	critical topographic slope for landsliding	–
C	6×10^4 kg m^{-1} s^{-2}	cohesion	1
Δt	10 years	time step	–
Δx	100 m	grid spacing	–
γ	2.7×10^4 kg m^{-2} s^{-2}	specific gravity	–
κ	0.01 m^2 yr^{-1}	di usivity	2,3
k_a	1.6×10^{-4} m^2 s^2 kg^{-1}	alluvial sediment transport coe cient	v.i.
k_b	1.2×10^{-7} m^2 s^2 kg^{-1}	bedrock incision coe cient	4, v.i.
k_w	8.0×10^{-4}	channel width coe cient	v.i.
Ω_0	4×10^5 kg s^{-3}	steam power threshold	v.i.
P	1 m yr^{-1}	precipitation rate	–
ϕ	17°	material friction angle	1
τ_r	500 years	earthquake recurrence interval	–

References: 1. Schmidt & Montgomery (1995); 2. Hanks *et al.* (1984); 3. Rosenbloom & Anderson (1994); 4. Stock & Montgomery (1995). v.i., visual inspection.

consider landscapes that develop in response to displacements on a single normal fault (Fig. 4a).

Experiments with a high-angle, planar normal fault

Experiment 1: Facets and spur benches

Figure 5 shows the landscape that develops during experiment 1, after 2000 kyr of run time. A well-defined and regularly spaced series of channels drain the mountain, and spurs between catchments are truncated, forming a set of triangular facets. Facets occur at a variety of spatial scales, from the dissected triangular shapes of entire spurs to low (<100 m), steep surfaces adjacent to the fault. Neighbouring spur crests in the middle of the footwall have grossly similar elevations and appear to form a concordant surface that dips toward the hangingwall, and that is incised or interrupted by the intervening catchments (Fig. 5). The landscape pictured in Fig. 5 is in steady-state; by this we mean that relief is not changing with time, and tectonic and surface processes are balanced at all points in the landscape. This is not to say that rates of erosion and rock uplift are everywhere the same, but that they are the same at all locations.

We define the landscape response time to be the time necessary for the along-strike catchment relief within the range – that is, the maximum relief across any one catchment, from valley bottom to ridge crest – to reach its maximum, steady-state value. The response time for landscapes at these spatial scales (≈ 10 km across) is of the order of several hundred thousand to one million years (Fig. 6). To assess how important the initial topography is in setting this landscape response time, we

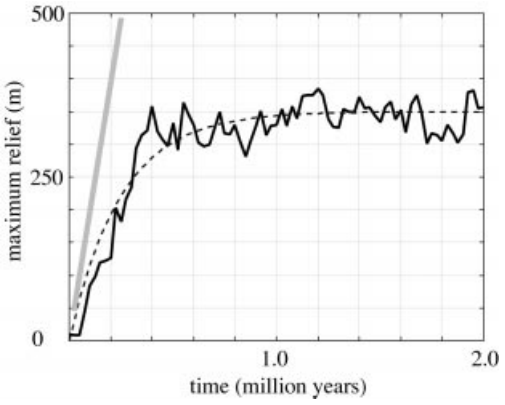

Fig. 6. Development of along-strike catchment relief – measured as the maximum di erence in elevation between a valley floor and the adjacent ridge crest – in experiment 1. The heavy grey line shows the accumulation of tectonic displacement at the range front, as dictated by the rate of fault slip; in the absence of any redistribution of mass by surface processes, this would correspond to the relief across the entire range at any time. The characteristic time to steady-state, as determined by fitting the relief curve to an exponential function, is of the order of 10^6 years shown as the thin dashed line.

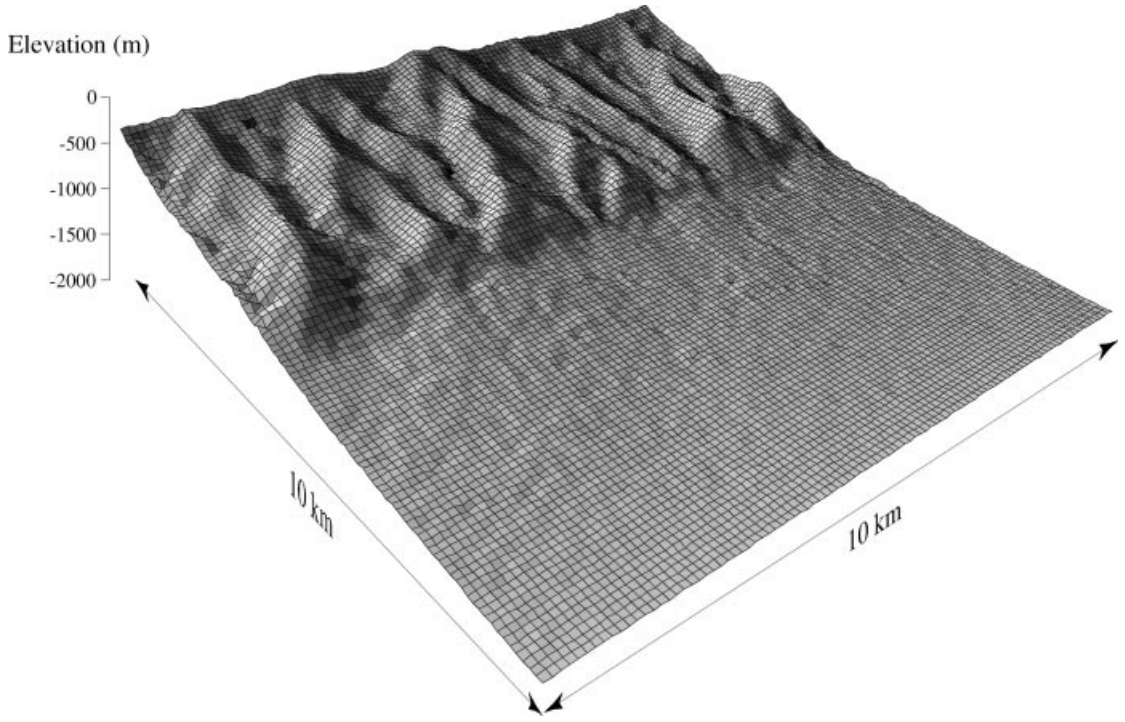

Fig. 5. Shaded-relief perspective view of topography from experiment 1, showing the steady-state landscape that develops after 2000 kyr of model run time under constant tectonic and climatic conditions. In this and in all subsequent plots, vertical exaggeration is 20 unless otherwise noted. Note the triangular facets and relatively straight and regularly spaced drainages. This view is similar to most range fronts in the Basin and Range province (e.g. Fig. 3a,d).

ran sensitivity experiments using identical parameters but di erent initial topographic conditions – in one case, a planar surface sloping toward the hangingwall at 1° and in another sloping away from the hangingwall at 1°. We found that the response time varies by less than an order of magnitude for radically di erent initial conditions. Once the landscape response time has passed, the topography is independent of its initial configuration. Thus, the 'memory' of those initial conditions will survive in the landscape for a finite but relatively short time.

Of particular interest to us are the features that caught the eyes of previous investigators, the most obvious of which is the triangular facet. It is clear that the facets developed here are not exhumed portions of the fault but that they are formed predominantly by landsliding. Densmore *et al.* (1998) demonstrated that some form of mass movement was necessary to produce facets; the much slower processes of regolith production and downslope transport are incapable of removing enough material from the hillslopes. As in the field, the model landscapes do not reveal this origin by the nature of deposits adjacent to the facets, for two reasons. First, landslide material is e ciently transported away from the facets by both the landslide-debris distribution algorithm (which unintentionally simulates a debris flow-like deposit) and by fluvial processes. Second and probably more importantly, the hangingwall is dropping fast enough that landslide materials, in fact all hangingwall deposits, are buried relatively quickly and covered by the continuously aggrading fluvial system (e.g. Friedmann *et al.*, 1994).

The combination of high uplift and erosion rates implies that facets, far from being static or remnant landforms, are extremely active. Despite this, individual facets are recognizable as distinct landforms for long periods of time. The facet form thus translates very e ciently through the footwall material as it is uplifted by tectonic displacement. We suggest that facets owe their very uniform slope (Menges, 1990) not to the dip of the exhumed fault plane but to the high e ciency of bedrock landsliding in responding to the monotonic fall in base level imposed by slip on the frontal fault, and to the existence of a well-defined rock mass 'angle of repose'. Their triangular shape is similarly maintained by bedrock landsliding in response to continued incision of the catchments on either side of the facet. In other words, it reflects the expected form of a strength-limited rock mass with falling base-levels on three sides.

In Hamblin's (1976) model of facet formation, the number of facets increases through time as the mountain front becomes steadily more dissected. Our experiments show that the number of recognizable facets remains remarkably constant through time as the landscape develops. Facet formation is clearly associated with periods of active fault displacement (Davis, 1903; Gilbert, 1928; Hamblin, 1976; Wallace, 1978). However, with the exception of the early model-years, prior to the achievement of a steady-state landscape, facet height remains relatively constant and does not reflect in a simple manner the rate of slip across the range-front normal fault.

The size and distribution of triangular facets are ultimately controlled by the drainage network that develops on the footwall, for three reasons. The locations of individual catchments define the locations of facets, and the spacing between catchments dictates the maximum relief on the facets in strength-limited landscapes. Also, rates of channel incision dictate the rate at which the facet form grows and evolves. Thus, processes which act to change or disrupt the footwall drainage network will necessarily a ect the facets as well; it is important to separate these influences on facet morphology from tectonic or climatic influences on the mountain front. For example, Fig. 7 shows closeups of part of the footwall from experiment 1. Despite the fact that the experimental topography is in steady-state, and that the along-strike catchment relief is unchanging, the form of the topography is far from static. Morphological changes at the mountain front, including the creation and removal of facets, are directly linked to drainage capture and reorganization events within the footwall block.

Hamblin's (1976) model of facet formation relied on the interpretation of a set of concordant benches within the footwall as periods of tectonic quiescence, during which the range front recessed leaving a low relief surface between the active fault and the front of the range. Our experiments also revealed a set of benches or spur crests in the middle of the footwall of grossly similar elevations along strike. In detail, the spur crests are made up of a series of subhorizontal benches, alternating with steeper segments (Fig. 8). We emphasize that this experiment used constant tectonic and climatic conditions, and that the spur benches represent a steady-state condition. We argue below that concordant spur crests and spur benches may owe their existence to strength-limited relief, the e cacy of landsliding and the establishment of a steady-state landscape.

Hillslope relief along strike is a function of the spacing of the major catchments and the distribution of hillslope gradients, which in turn depends on the rock mass strength (Schmidt & Montgomery, 1995). The major catchments have similar drainage areas and feel essentially the same base-level fall in each model earthquake; thus the long profiles of the major catchments are very similar in shape and elevation along strike. Since the hillslopes respond very quickly to changes in channel bed elevation (Densmore *et al.*, 1998), and since the relief is limited by catchment spacing, it follows that similar elevations in the channel bed should lead to similar elevations in the spur crests. Thus the concordant spur crest elevations directly reflect the channel bed elevations. This concordance breaks down in two areas – near the fault, on the facets, where the hillslopes respond to tectonic as well as fluvial control of local base-level; and in the channel headwaters, where fluvial incision is relatively minor and the relief is not limited by the channel spacing. The spurs are not simple triangular prisms, however, because the major catchments branch and have some along-strike width. Where those branches have impinged upon the

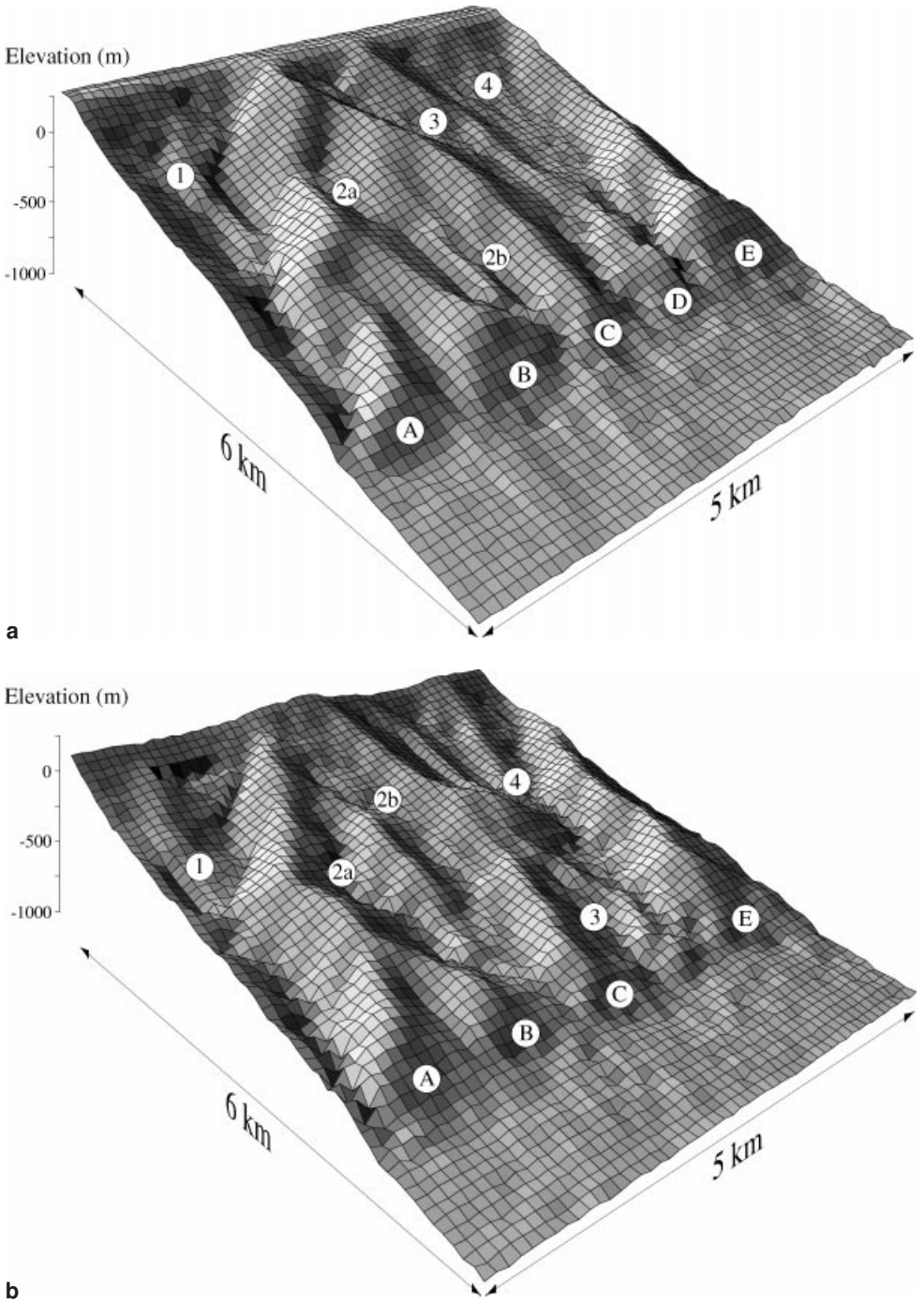

Fig. 7. Shaded-relief perspective views of part of the footwall from experiment 1 at four di erent times during the experiment, showing how drainage capture and reorganization a ects the morphology of the mountain front. The numbers (1, 2a, 2b, 3 and 4) mark individual catchment, while the letters (A, B, C, D and E) mark triangular facets. Catchments 2a and 2b are tributaries within a single larger drainage basin. (a) Topography after 1000 kyr of model run time; (b) after 1325 kyr; (c) after 1350 kyr; (d) after 2000 kyr. The upper portion of catchment 3 is captured by catchment 4, which removes facet D. Also, the continuing competition for drainage area within the footwall causes changes in the relative sizes of catchments 2a and 2b, which results in the eventual removal of facet B.

spurs, the elevation of the spur crest is lowered by fluvial incision and subsequent landsliding. This lowering gives rise to a spur top that is generally smooth and shallowly dipping, but that is broken into a set of discrete benches where nearby channels have lowered the spur elevation (Fig. 8).

Experiments 2 and 3: piedmonts

It is not uncommon to find in the Basin and Range a plane of low-relief or piedmont that skirts part or all of the range and whose border yields an embayed range front. This issue was tackled by Davis (1903) who

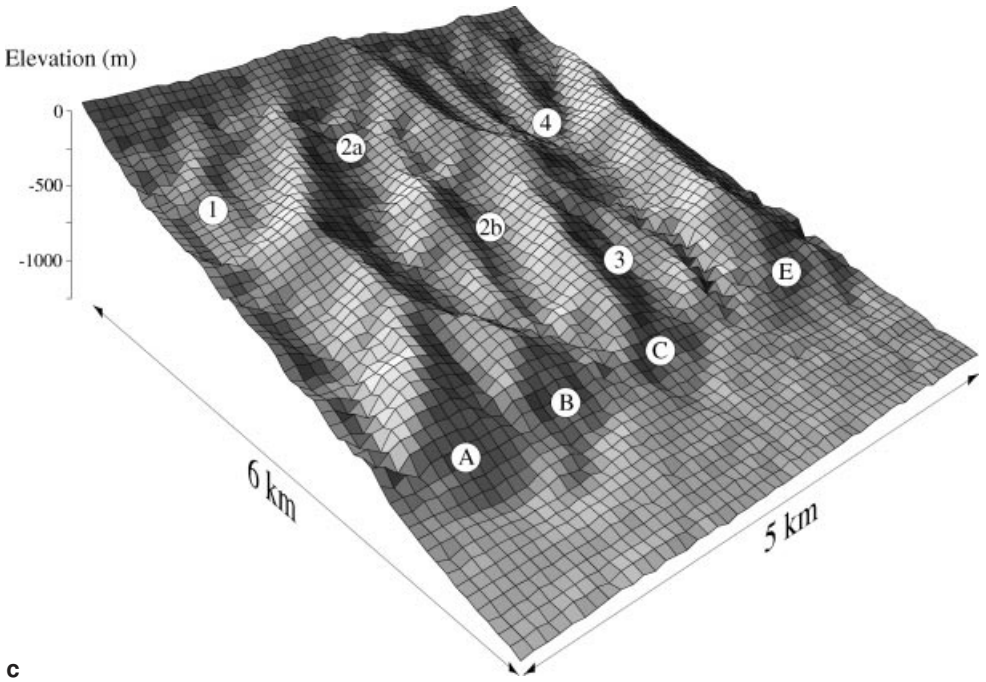

c

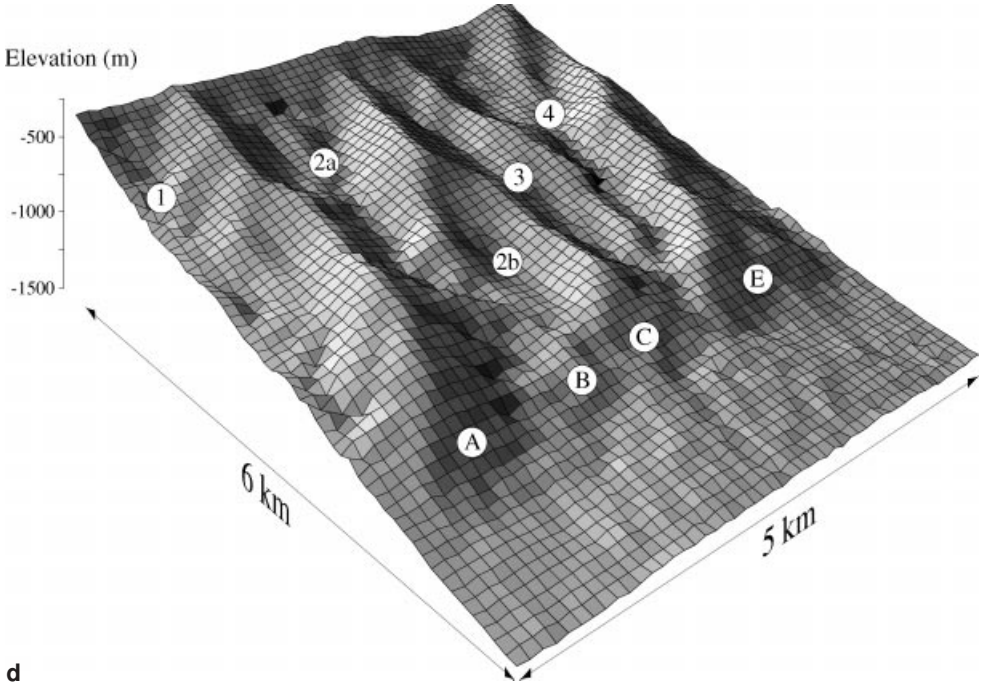

d

outlined a conceptual model of range development in which the cessation of activity along a range-bounding fault, and the consequent base-level stability, leads to embayment of the mountain front and alluviation of the valleys. We test this model directly in experiment 2 by turning o the fault, using the topography from experiment 1 as the initial condition, and allowing the landscape to evolve strictly by surface processes.

Figure 9 shows the resulting landscape after 250 kyr of model time. The catchments are extensively alluviated well into their upper reaches, creating large embayments in the mountain front. A low-relief alluvial surface extends smoothly across the fault. In cross-section, the alluvial fill is <500 m thick on the footwall block, but abruptly increases to 1000–2000 m thick on the hanging-wall block (Fig. 10). Evidence of subsurface faulting, such as this abrupt transition in alluvial thickness, may thus persist long after activity on that structure has ceased. As shown by the smooth, continuous alluvial surface across the inactive fault trace, there is still active sediment transport across the fault and onto the hanging-wall block. This surface, despite its low relief and abrupt contact with the steep, exposed bedrock of the footwall, is therefore not a pediment in the classical sense

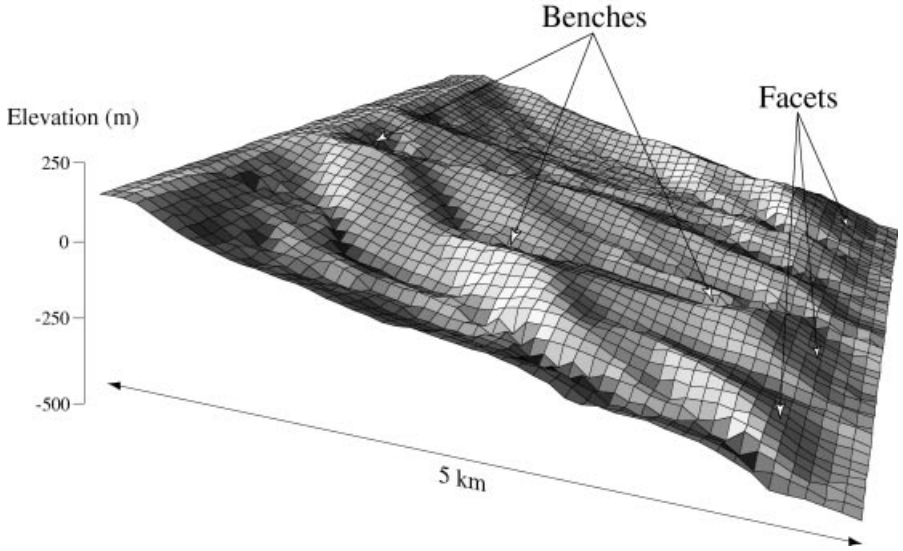

Fig. 8. Shaded-relief perspective view of part of the footwall from experiment 1 after 1000 kyr of model run time. Note the horizontal ridgetops or benches, forming a concordant surface, similar to those observed by Hamblin (1976) and observed in many range fronts in the western USA. Similar features are also seen in Fig. 3(b) and Fig. 5. Both tectonic and climatic conditions were held constant during this model run.

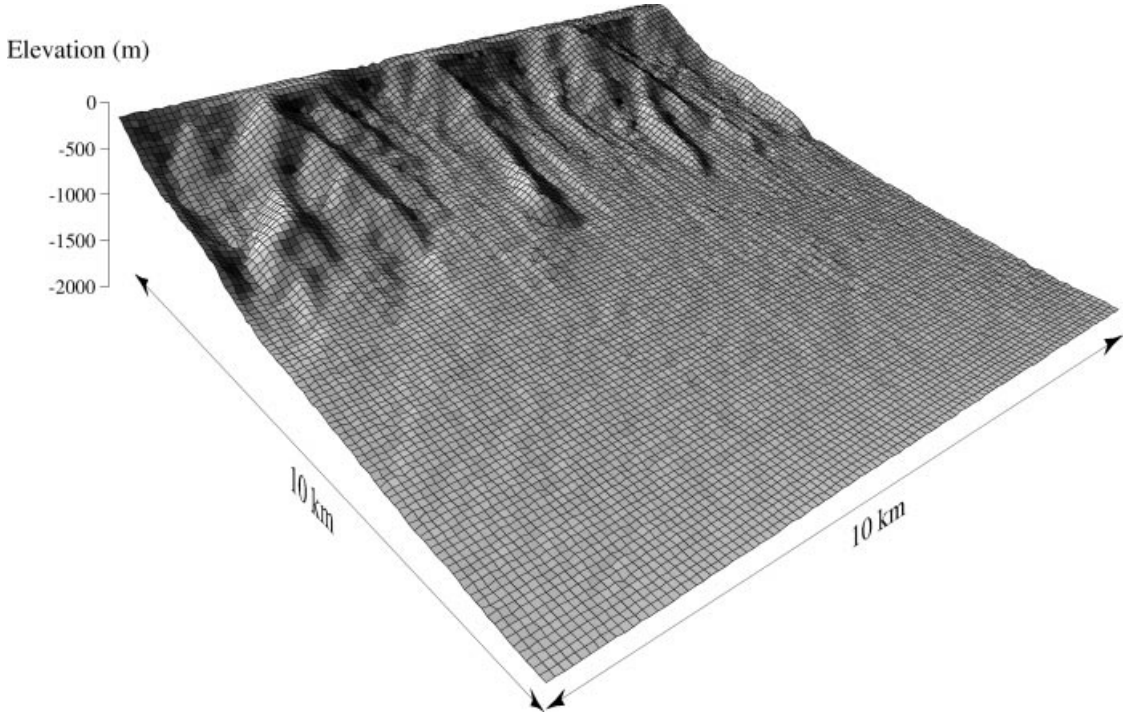

Fig. 9. Shaded-relief perspective view of experiment 3, 250 kyr after turning the tectonic displacements o . Note that the range front becomes alluviated and consequently embayed and that the remnants of the spurs and facets bear some resemblance to Davis' monticules (Davis, 1925).

(Dohrenwend, 1994); the surface is depositional rather than erosional, a zone of slow aggradation rather than transport. Wallace (1978) used this morphology as evidence that the fault along the east side of the Humboldts, while perhaps active in the late Cenozoic, has been inactive for some time. Our experimental results are consistent with that interpretation.

We explore the evolution of a piedmont further by again taking as the initial condition the topography after experiment 1 and stepping the fault 2 km further into the basin (experiment 3). In other words, we are simulating a migration of the faulting into the hangingwall, a process which we infer from observation in various parts of the northern Basin and Range and which has been proposed by Wernicke & Axen (1988) to generate individual mountain ranges in the central Basin and Range.

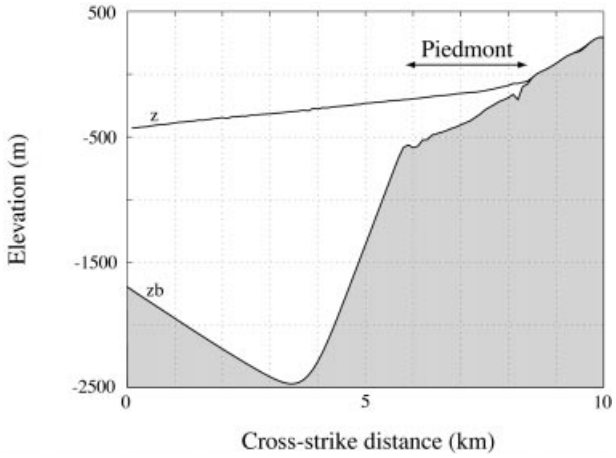

Fig. 10. Fault-perpendicular cross-section through the centre of the experiment 3 landscape. The line marked 'z' is the surface topography, and the line marked 'zb' is the bedrock topography. Note the broad alluviated piedmont on the footwall.

Figure 11 shows the topography developed during experiment 3 after 250 kyr of model run time. Basin deposits in the footwall of the new fault have been uplifted and incised, forming a broad, low-relief surface. The density of channels draining this new footwall block is high, reflecting the fact that the channels are cut into easily erodible fan sediment. Catchments within the original footwall block have alluviated, a somewhat unexpected result. This alluviation occurs because those channels originally achieved equilibrium profiles with respect to continuous base-level fall that was localized along the old fault trace. After the fault steps out, base-level continues to fall at the same rate, but the topographic gradient between all points within the catchment and the locus of base-level fall has decreased. The channel therefore lacks the power necessary to maintain its profile, and responds by alluviating its valley. Not until the knickpoint that will have been generated at the new base-level fall (i.e. along the trace of the new fault) has migrated to the position of the older fault trace will these channels again be able to incise. And these channels should be incising into a fill terrace, the downstream extent of which will mark the location of the older fault.

Interestingly, with our current set of parameter values much of the topographic evidence for the old fault trace has been lost by 250 kyr. In fact, after 500 kyr of model run time, it is very di cult to discern the location of the old fault trace by using topography alone. While the parameter values we use are uncertain to at least an order of magnitude (Densmore *et al*., 1998), we note that this notion of rapid topographic change is consistent with our observations of high activity and rapid resurfacing of the mountain front (Densmore *et al*., 1998).

The broad, slightly dissected surface that develops between the fault traces is highly reminiscent of the pediment sequence formed on basin deposits on the west side of the Ruby Mountains (surface 2 of Sharp, 1940). Fault activity has shifted from the base of the Rubys to a point several kilometres to the west, though the timing of this shift is poorly known.

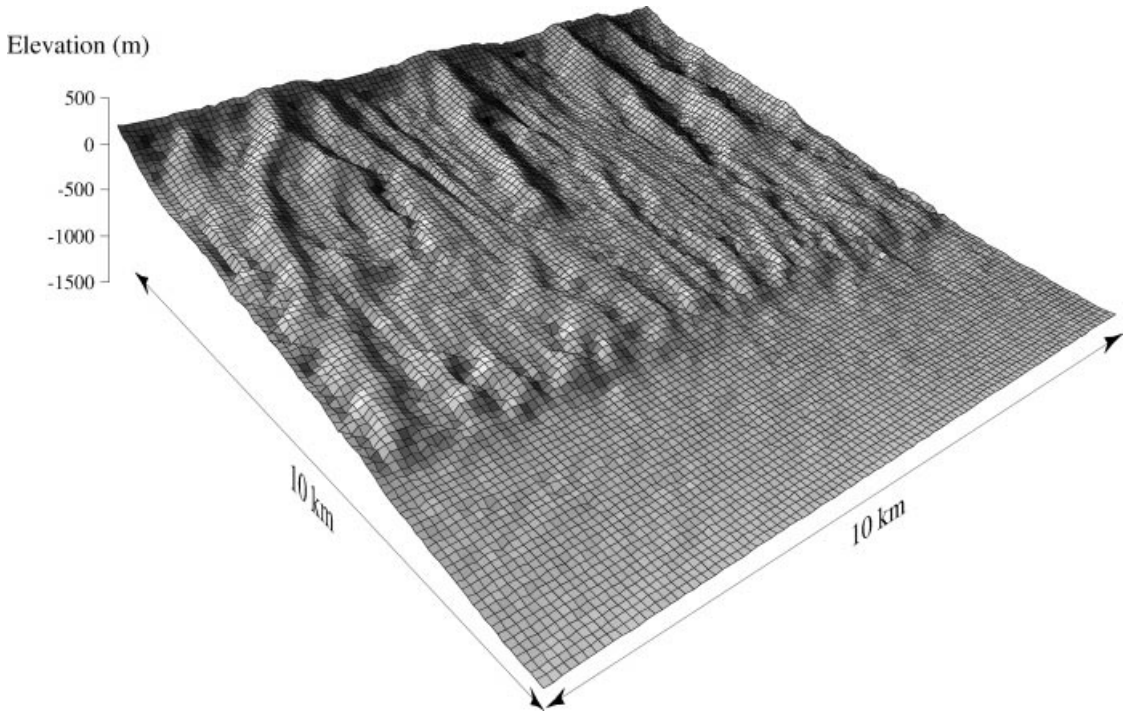

Fig. 11. Shaded-relief perspective view of topography from experiment 2, 250 kyr after the active fault steps 2 km into the original hangingwall. Note the uplifted and incised bajada, the alluviated channels on the original footwall and the high drainage density of channels within the sediments of the new footwall. Similar morphologies are observed along the eastern edge of the Ruby Mountains, along the western edge of the Toiyabe Range and in many places in central Nevada.

Experiments with a horst

Crustal extension over a large fraction of the central northern Basin and Range (central Nevada) is accommodated by normal faults whose dips alternately oppose each other, which gives rise to the set of parallel, north–south trending horsts, Dutton's army of caterpillars (Dutton, 1880). The average spacing between these range-bounding faults is about 10–15 km, which reflects the thickness of seismogenic crust, such that a single fault is able to accommodate the incremental build up of elastic strain energy over a length scale that is the width (down-dip extent) of the fault. The faults are thus interdependent and so too will be the topography etched into the rising horsts. Thus we next consider a set of experiments driven by the surface displacements on two normal faults with opposing dips (Fig. 4b). While such a range could be created by juxtaposing two landscapes from the single-fault experiments back to back, interesting competitions and landforms arise from allowing the landscape to evolve under the influence of both faults simultaneously.

Experiments 4 and 5: a horst

Figure 12 shows the topography from experiment 4 after 2000 kyr of model run time. The initial topography was a symmetric inverted V, with the crest parallel to and centred between the faults, and with a dip of 1°. Displacement rates across both faults is the same. Channels in the footwalls have incised headward from either side of the crest, first interacting $\approx$1500 kyr into the run. The crest and the drainage divide are coincident; the position of the crest is dictated by the locations of the major catchments on both flanks of the range. A large catchment on one side will e ciently incise headward, enlarging itself and pushing the drainage divide toward the other flank. This gives rise to the slightly arcuate pattern seen in Fig. 12.

The symmetrical initial conditions used in experiment 4 are unlikely to occur in real geological settings. It is more likely that some pre-existing topography will be present, and will impose an inherited slope and drainage pattern on the landscape, albeit perhaps only lightly etched into it. The channel system that arises in response to tectonic motion on the horst bounding faults must therefore overcome or assimilate this inheritance. To investigate the role of inherited topography, we ran additional experiments with a monotonic 1° initial slope across the model space (experiment 5). We found that this initial topography controlled the early positions and drainage directions of the catchments, but that it was very quickly overwhelmed by the topography imposed by tectonic displacements. By the time the catchments on either side of the range interact, the topography of the range is statistically indistinguishable from that of experiment 4.

Experiments with microclimate

Experiment 6: orographic precipitation

The development of topography may be profoundly a ected by spatial and temporal variations in microclimatic, as well as tectonic, processes. Much of the precipitation that currently falls on the Basin and Range is supplied by air masses that travel from west to east across the region. As this air is forced up and over individual ranges, it loses its capacity to carry moisture, leading to precipitation rates that increase monotonically with elevation. By the time the air mass reaches the leeward side of the range, its moisture is significantly depleted, producing more arid conditions along the eastern faces of many of the larger ranges. These conditions (and knowingly

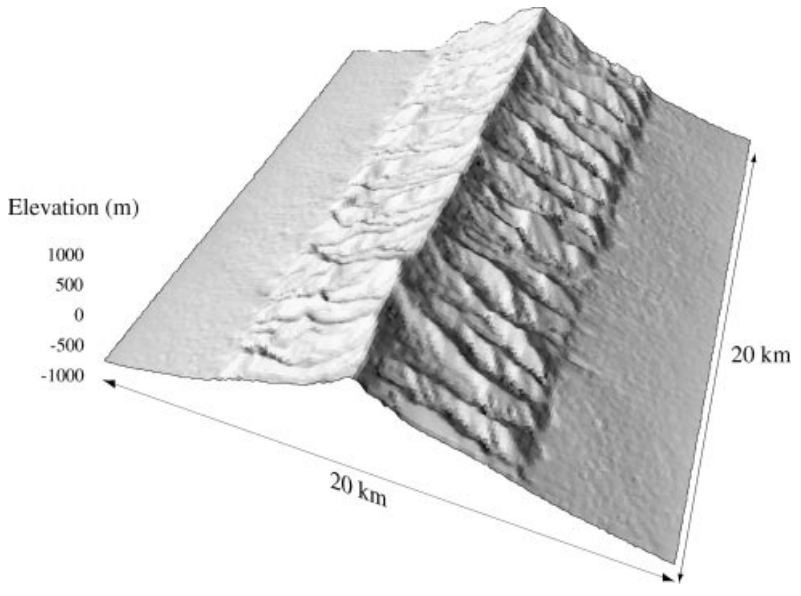

Fig. 12. Shaded-relief perspective view of experiment 4, showing the topography that results from 2000 kyr from a simple horst fault geometry with symmetrical tectonic and geomorphic conditions. Initial topography was an inverted V, with 1° side slopes.

neglecting evapotransiration) should decrease the available stream power and thus decrease the amount of geomorphic work done by the channel network.

To test this hypothesis, we applied an asymmetric precipitation pattern (Fig. 13, inset) to the topography derived in experiment 4, and allowed this experiment, experiment 6, to run for 1000 kyr. Precipitation was taken to be constant over each hangingwall, and increased linearly with elevation over the footwall block to a maximum at the crest of the range. The precipitation maximum was fixed to the topographic crest, and thus migrated with the crest through the experiment. The resulting landscape is shown in Fig. 13. Higher precipitation on the windward side of the range increases the stream power of catchments draining that side of the range, leading to high drainage density and sediment transport. With the values of threshold stream power and sediment transport parameters used in the experiment, this large sediment flux from the windward footwall overwhelms the available accommodation space, leading to the deposition of a thick sedimentary package on the windward hangingwall. Base-level for the windward catchments is thus several hundred metres higher than it is for the leeward catchments. This has the e ect of reducing the power of channels on the windward side, allowing the leeward catchments to grow at their expense. This rather counterintuitive result is an example of a negative feedback in this relatively complex (but still simplified) model environment. If, for example, material eroded from the windward flank of the range was transported out of the system (by an axial drainage system), base-level would remain fixed and the increased discharge and hence power of the windward channels would then drive their headwaters, and eventually the range divide, back toward the leeward side. The early part of this scenario might well see the larger channels on the windward flank breach the divide so that they begin to capture drainage while it is still on the leeward side of the range. A possible example of this is seen along the Ruby Mountains in north-eastern Nevada where several rivers that drain the western side (the windward side) of the range have broken through the main divide (Sharp, 1940).

DISCUSSION

We have shown above that many of the characteristics in common among the mountain fronts and piedmonts in the Basin and Range may be reproduced by a fairly simple, steady combination of tectonic and surface processes. Where these processes do vary, either in space or in time, interesting and sometimes counterintuitive landscapes result. A benefit of the experiments presented here lies in the unexpected issues that they raise and in the ability to explore the results of coupling between the modelled processes. We discuss these issues below.

Facets

We concur with previous studies that link facet formation with periods of active fault displacement (Hamblin, 1976; Wallace, 1978). We view facets, however, as secondary landforms that owe their size and shape to the rock strength and to spacing between the incising channels that bound them, and we see no evidence that facet height should correspond to fault slip-rate. In contrast, the combination of high uplift and erosion rates implies that facets, far from being static or remnant landforms, are extremely active. Despite this, individual facets are recognizable as distinct landforms for long periods of time. The facet form thus translates very e ciently through the footwall material as it is uplifted by tectonic

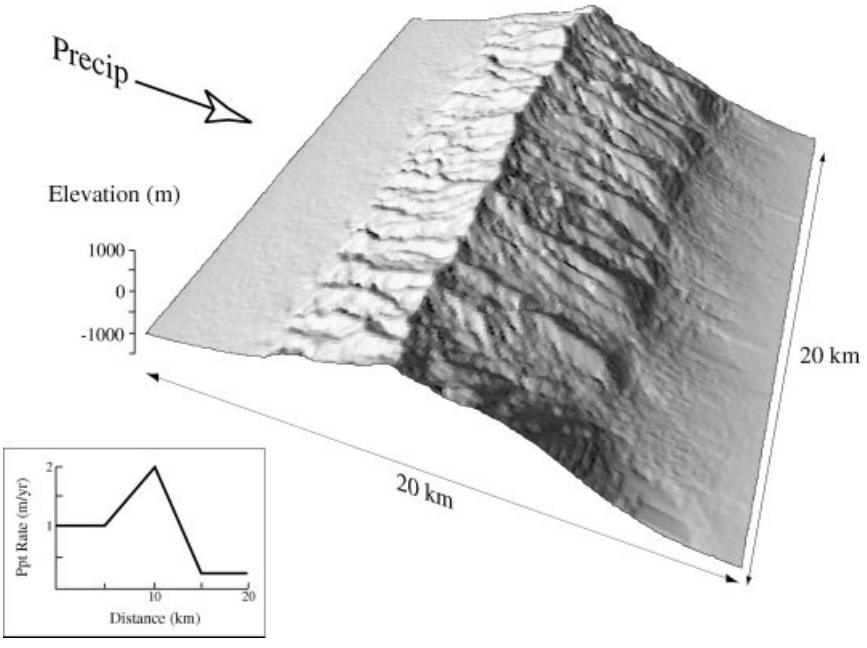

Fig. 13. Shaded-relief perspective view of experiment 6, showing the topography that results from a symmetrical tectonic displacement field and an asymmetrical precipitation field (inset). The model was run for 1000 kyr, and the initial topography was the steady-state horst of Fig. 12.

displacement. We suggest that facets owe their very uniform slope (Menges, 1990) not to the dip of the exhumed fault plane but to the high e ciency of bedrock landsliding in responding to the monotonic fall in base-level imposed by slip on the frontal fault. Their triangular shape is similarly maintained by bedrock landsliding in response to continued incision of the catchments on either side of the facet.

While facets are generally not exhumed or preserved fault planes and do not directly reflect the dip of the fault, a very small fraction of facets that have yet to fail through landsliding may retain parts of the fault plane (e.g. part of the Genoa fault scarp along the eastern face of the Sierras, near Carson City, Nevada). A further exception will exist in regions of low-angle normal faulting, since low surface slopes discourage landsliding and limit the availability of stream power. Examples include parts of the west-facing flanks of the Panamint Range and possibly the turtleback surfaces that comprise the Death Valley normal fault (Wright *et al*., 1974; Holm *et al*., 1994). In general, however, facets serve as indicators of the maximum slope and height of stable hillslopes, and thus of the rock mass strength (Schmidt & Montgomery, 1995).

The model of facet and spur-bench development outlined above presupposes that the landscape is able to achieve a quasi-steady state, strength-limited topography, as we have observed in our experiments. The achievement of steady-state, however, may be the Holy Grail of geomorphology, as complexities in the system provide what is essentially a moving target of what is steady-state. For example, various lithologies may be encountered as the footwall emerges, climate changes may oscillate at a frequency that is faster than the response time of the prevailing processes, the deformation may field may change relatively rapidly, etc. These types of complexities will yield a dynamic topography in the sense that a steady-state may never be acheived.

Piedmonts

While we cannot rule out the process of parallel scarp retreat as envisaged by Hamblin (1976), we see no evidence for it in our experiments. It appears that, with reasonable geomorphic process rates, any weathering and backwearing of the mountain front is overwhelmed by the continual sediment flux supplied to the piedmont by landsliding and fluvial transport (Blair & McPherson, 1994; Densmore *et al*., 1998), even when the rangefront fault is inactive. The mountain front is thus buried in its own waste, after the conceptual model of Davis (1903). Even in cases where sediment supply from the footwall is limited, we argue below that parallel slope retreat requires some mechanism to remove weathered material from the mountain front, in order to maintain the existing topography.

A spatial shift in the locus of tectonic activity onto splay faults has been documented for several range-bounding faults (Doser, 1985; Bell & Katzer, 1987; Bruhn *et al*., 1987; Hodges *et al*., 1989; Miller, 1991). Several workers have presented mechanical arguments for the transfer of slip onto structures in the hangingwall of an active normal fault, based on rotation of the fault plane into attitudes unfavourable for continued slip (Wernicke & Axen, 1988; Forsyth, 1992). Such a transfer will produce a gap between the active fault and the mountain front, potentially leading an observer to call on parallel retreat of the mountain front to explain the gap.

Experiment 3 documents the formation of low-relief surfaces that are thinly sediment-mantled relative to the hangingwall basin. But these surfaces are clearly not pediments as presented by Dohrenwend (1994) and others. The processes by which pediments form are largely unknown, though most recent work has focused on the role played by the expansion and integration of footwall drainage basins, giving way in the endgame to weathering-limited di usion of the interfluves (Dohrenwend, 1994). We suggest that some of the voluminous debate over pediments and pediment processes represent misguided attempts to shoehorn many low-relief piedmonts into a single genetic classification. For example, the landscape in experiment 3 exhibits some classical pediment features; the piedmont is very low-relief, the junction between the piedmont and the mountain block is sharp but highly arcuate, and palaeo-mountain peaks are exposed as inselbergs (the 'monticules' of Davis, 1925) poking above the alluvial fill (Fig. 9). These results may be consistent with the evolution of pediments that are formed on old fan materials, such as the Lee surface on the west side of the Ruby Mountains (Sharp, 1940). There, the boundary between old fanglomerate 'bedrock' and younger alluvium may be indistinct. However, these results do not account for the evolution of pediments formed on more resistant, crystalline bedrock, nor those whose alluvial cover truly is thin or nonexistent.

Strength and incision-limited landscapes

Experiment 1 provides an insight into the behaviour of a 'steady-state' mountain front – that is, one in which the controlling tectonic and climatic patterns and rates are unchanging, and the spatial extent of the range is fixed. Along such a front, we distinguish two distinct morphological regimes. Near the front, the hillslope relief between the spurs and catchments is dictated by the catchment spacing and the bedrock strength, which is an example of a strength-limited landscape (Densmore *et al*., 1998). Hillslope relief is independent of rates of both tectonic uplift and catchment incision, as long as uplift continues; rock strength limits the relief.

In contrast, near the crest of the range the relief is dictated by the degree of fluvial incision into the footwall, which is in turn a function of the available stream power. Hillslope relief generation in this regime is thus incision-limited. This distinction between strength-limited and

incision-limited relief makes possible the spatial mismatch between areas of high elevation and areas of high uplift rate. The highest relative uplift rates along a normal fault-bounded mountain front are found in the footwall, immediately adjacent to the fault (Fig. 12). However, elevation and hillslope relief are kept relatively low, as high values of stream power allow fluvial erosion and subsequent bedrock landsliding to e ciently denude the footwall. Higher up in the footwall, low stream power leads to low incision rates, allowing even small values of tectonic uplift to produce considerable topography. The mountain front achieves a steady state wherein both the overall relief and the hillslope relief reflect a delicate balance between stream power, rock strength and tectonic uplift.

The role of initial conditions

We have limited the exploration of initial conditions to relatively simple, gentle initial topographies. Clearly, the influence of any initial topography on the form of a growing mountain range will depend strongly on the rates of tectonic and geomorphic processes which shape the range. The faster these rates are, the higher the flux of material through the 'mountain mill', and the more rapidly the initial conditions are forgotten (e.g. Anderson *et al.*, 1999). An important issue to consider is the quantitative measure of the landscape that is used to assess this memory – that is, what variable should be used to discriminate between initial and final landscapes, and to evaluate the relative contribution of each to the topography at any one instant? This is still a matter of some debate, despite e orts by Willgoose (1994) to develop a simple statistic for characterizing topography. While we have not employed Willgoose's approach (which was designed for a di usion-only landscape evolution model), we note that even relatively simple measures of the landscape, such as maximum relief and hypsometry, may prove useful in distinguishing between di erent numerical experiments (e.g. Densmore *et al.*, 1998), and indeed between the relative roles of di erent processes in shaping topography. For example, Densmore & Hovius (1998) suggested that the spatial distribution of steep slopes was similar to the spatial distribution of landslides triggered by climatic processes in some active mountain belts, allowing them to define climatic events as the important short-term cause of large-scale landsliding and sediment production.

Climate signatures in landscapes

We have demonstrated that the landscape response time is of the order of 10^5 years, which means that landscapes will or may retain information about causative factors that occur with a frequency of less than several hundred thousands of years. There are an increasing number of studies that suggest the ≈ 100 kyr glacial periodicity during the Quaternary may have a profound e ect on landscapes (e.g. Molnar *et al.*, 1994). Our results suggest that such periods of climate change should leave fingerprints in the landscape (cf. Rinaldo *et al.*, 1995). To explore this more fully, we need to better couple climate and surface processes. The current version of *Zscape* couples surface processes to the extent that hillslope and channel processes both depend on slope and discharge, hence there is some tie to climate also. Climate is only tentatively linked to landslides, however, to the extent that channel incision is an important factor in driving landslides and incision is driven by available stream power. Further coupling to climate would incorporate the use of pore fluid pressures within the rock mass, which requires a rule set that governs the rate of infiltration of precipitation, plus some parameterization of fracture permeability within the rock mass.

We have performed some very preliminary experiments in which the probability of landsliding varies directly with the precipitation rate, with a constant of proportionality varying from 1.0 to 0.1. With a constant of 1.0, if the precipitation rate falls 50%, so does the probability of a landslide occurring at any particular node; with a constant of 0.1, a similar change in precipitation rate yields only a 20% reduction in probability. This admittedly very simplistic rule, when combined with a precipitation rate that varies sinusoidally over time, yields landscapes in which the catchment-averaged footwall erosion rates vary almost exactly with changes in precipitation; there is no lag between peaks in precipitation rate and peaks in footwall erosion rate (P. A. Allen and A. L. Densmore, manuscript in preparation). In addition, the catchments in these landscapes are characterized by steep gorges that form during times of low precipitation. During these periods, channel incision still occurs in response to continued fault activity and base-level lowering, but landslide probabilities are low and so relatively little material is removed from the hillslopes. These steep gorges are strongly reminiscent of the classic wine-glass canyons visible in some Basin and Range range fronts, the best example of which may be the west flank of the Black Mountains facing Death Valley.

Coupling of faulting and surface processes

An interesting issue raised by the experiments involves the interaction of faulting processes via the spatial scale of surface processes. For example, fluvial systems that drain several or many fault blocks (e.g. East Humboldt River in northern Nevada or tributaries to the Snake River, southern Idaho) may e ectively communicate tectonic or climatic changes from one place to another. Thus, if a drop in base-level occurs at a downstream location whether caused by tectonic and climatic processes, it will in time be communicated further upstream where its e ect may be to generate a signature (e.g. incision, possibly the generation of fluvial terraces) in the landscape that is related to conditions far removed from the local setting. If, alternatively, the fluvial system is spatially confined, perhaps for tectonic reasons, it is

possible that eroded material essentially chokes the drainages, reducing local stream gradients and thus their power, therefore slowing the rate of erosion (experiment 5). Again, such a geomorphic signature may have more to do with the spatial scale of the fluvial system (i.e. whether the local system is open or closed to mass loss) than with the intrinsic tectonics. Such a scenario may be pertinent to the Neogene evolution of the Wasatch fault and associated basins (King & Ellis, 1990; Kusznir & Westaway, 1990).

These scenarios and many others that could be conceived point to the di culty of interpreting geomorphic signatures within landscapes in terms of tectonics or climate (e.g. England & Molnar, 1990), but the present LEM provides a potentially powerful tool to explore these types of scenarios with reproducible and physically based rigour.

CONCLUSIONS

We produce characteristic landforms observed in the Basin and Range using a simple and temporally invariant set of tectonic and geomorphic rules. Particular conclusions are that facets are generally not exhumed fault planes, but are continually resurfaced during periods of active fault slip. Continual slip and base-level drop leads to the development of steady-state channel profiles and thus steady-state landscapes, as hillslopes respond rapidly to channel incision. This leads to concordant ridgecrests and the appearance of a bench. The position of the main drainage divide, which may or may not be coincident with the range crest, reflects the competition for drainage area between channels on opposite sides of the crest. When the crest and drainage divide are not coincident, we may have interesting things to say about asymmetries in the initial conditions and/or forcing. We have demonstrated that even with the relative simplicities employed in these experiments, there are still enough fundamental processes that may be contrived in a number of reasonable ways to produce unexpected results. The various but still limited scenarios examined here yield landscapes that are the results of both tectonic and erosional processes and depending at which point in time we choose to examine them, one of these processes may appear to be the dominant and causative process. We suggested earlier that most of what we know about Basin and Range topography we knew at the turn of the nineteenth century, thanks to the impressive observations made by geologists at the time. The value of the experiments presented here is to demonstrate that these observations are reproducible using a relatively simple description of the relevant physics and that we can recognize and explain various landscape morphologies that have in the past been the subject of purely qualititative reasoning.

ACKNOWLEDGMENTS

We thank Ramón Arrowsmith, David Montgomery and Sean Willett for constructive and insightful reviews, Ed Boring for computer assistance, and Paul Bodin, Niels Hovius and Brian McAdoo for helpful discussions. Supported by a NASA Topography and Surface Change grant to M.A.E. and R.S.A., and by a NASA Earth System Science Graduate Fellowship to A.L.D. CERI contribution number 350.

REFERENCES

A , F. (1970) Brief description of a comprehensive three-dimensional process-response model of landform development. *Z. Geomorphol.*, **24,** 11–22.

A , R.S. (1994) Evolution of the Santa Cruz Mountains, California, through tectonic growth and geomorphic decay. *J. Geophys. Res.*, **99,** 20161–20179.

A , R.S., D , A.L. & E , M.A. (1999) The generation and degradation of marine terraces. *Basin Res.*, **11,** 7–19.

A , R.S., D , G.S. & D , A.L. (1994) Sediment fluxes from model and real bedrock-channeled catchments: responses to baselevel, knickpoint and channel network evolution. *Geol. Soc. Am. Abstr. Prog.*, **26,** 238–239.

A , R. S. & H , N.F. (1989) Interaction of weathering and transport processes in the evolution of arid landscapes. In: *Quantitative Dynamic Stratigraphy* (Ed. by T.A. Cross), pp. 349–361. Prentice Hall, Englewood Cli s, NJ.

B , R.A. (1977) Bed load transport by natural rivers. *Water Resour. Res.,* **13,** 303–312.

B , J.M. & W , B.P. (1984) The Snake Range decollement interpreted as a major extensional shear zone. *Tectonics*, **6,** 647–657.

B , C., F , P. & H , J. (1991) Erosional control of active compressional orogens. In: *Thrust Tectonics* (Ed. by K.R. McClay), pp. 1–18. Chapman & Hall, New York.

B , J.W. & K , T. (1987) Surficial geology, hydrology, and late Quaternary tectonics of the IXL Canyon area, Nevada. *Bull. Nev. Bur. Mines Geol.*, **102**.

B , P.R. (1994) Using in situ produced cosmogenic isotopes to estimate rates of landscape evolution: a review from the geomorphic perspective. *J. Geophys. Res.*, **99,** 13885–13896.

B , P. (1989) New finite element techniques for modeling deformation histories of continents with stratified temperature-dependent rheology. *J. Geophys. Res.*, **94,** 3967–3990.

B , T.C. & M P , J.G. (1994) Alluvial fan processes and forms. In: *Geomorphology of Desert Environments* (Ed. by A.D. Abrahams & A.J. Parsons), pp. 354–402. Chapman & Hall, London.

B , R.L., G , P.R. & P , W.T. (1987) Seismogenic characteristics of the Salt Lake segment, Wasatch normal fault zone. In: *Special Volume on Continental Extensional Tectonics* (Ed. by M.P. Coward, J.F. Dewey & P.L. Hancock), *J. Geol. Soc. London*, **28,** 337–353.

B , W.R. (1988) Flexural rotation of normal faults, *Tectonics*, **5,** 959–973.

B , B.C., H , K.V. & R , L.H. (1987) Geology of Panamint Valley-Saline Valley pull-apart system, California: palinspastic evidence for low-angle geometry of a Neogene range-bounding fault. *J. Geophys. Res.*, **92,** 10422–10426.

B , J.O.D., S , R.B. & G , J.W. (1994) The Teton fault, Wyoming: Topographic signature, neotectonics, and mechanisms of deformation. *J. Geophys. Res.*, **99,** 20095–20122.

C , S.J. & W , S.G. (1998) Geologic evidence for low dip on the historically active Dixie Valley fault, central Nevada. *EOS, American Geophysical Union Transactions*, **79,** F875.

D , W.M. (1903) The mountain ranges of the Great Basin. *Harv. Coll. Mus. Comp. Zoo. Bull.*, **42,** 129–177.

D , W.M. (1925) The Basin Range problem. *Proc. Nat. Acad. Sci.*, **11,** 387–392.

D , A.L., A , R.S., M Adoo, B.G. & E , M.A. (1997) Hillslope evolution by bedrock landslides. *Science*, **275,** 369–372.

D , A.L., E , M.A. & A , R.S. (1998) Landsliding and the evolution of normal fault-bounded mountains. *J. Geophys. Res.*, **103,** 15203–15219.

D , A.L. & H , N. (1998) The topographic fingerprint of bedrock landsliding. *EOS, Fall Meeting Supplement*.

D , T.H., R , S., L , J. & R , M.C. (1995) Constraints on present-day Basin and Range deformation from space geodesy. *Tectonics*, **14,** 755–772.

D , J.C. (1994) Pediments in arid environments. In: *Geomorphology of Desert Environments* (Ed. by A.D. Abrahams & A.J. Parsons), pp. 321–353. Chapman & Hall, London.

D , D.I. (1985) Source parameters and faulting processes of the 1959 Hebgen Lake, Montana, earthquake sequence. *J. Geophys. Res.*, **90,** 4537–4555.

D , D.I. & S , R.B. (1989) An assessment of source parameters of earthquakes in the Cordillera of the western United States. *Bull. Seismol. Soc. Am.*, **79,** 1383–1409.

D , C.E. (1880) *Geology of the high plateaus of Utah*. U.S. Geog. & Geol. Surv. Rocky Mtn. Reg.

E , G.P. (1982) The Basin and Range province: Origin and tectonic significance. *Annu. Rev. Earth Planetary Sci.*, **10,** 409–440.

E , P.K., S , R.B. & R , C. (1987) Kinematics of Basin and Range intraplate extension In: *Continental Extensional Tectonics* (Ed. by M.P. Coward, J.F. Dewey & P.L. Hancock), *Geol. Soc. Spec. Publ.*, **28,** 371–392.

E , M.A. (1991) Tectonics and topography in regions of active extension: examples from the basin and range. *EOS*, **72,** 497.

E , P.C. & M , P. (1990) Surface uplift, uplift of rocks, and exhumation of rocks. *Geology*, **18,** 1173–1177.

F , N.M. (1928) *Physiographic divisions of the United States*, 3rd edn. Ann. Assoc. Am. Geog.

F , D.W. (1992) Finite extension and low-angle normal faulting. *Geology*, **20,** 27–30.

F , S.J., D , G.A., F , T.K., B , T., P , M., B , D.W. & B , B.C. (1994) Stratigraphy and gravity-glide elements of a Miocene supradetachment basin, Shadow Valley, East Mojave Desert. In: *Geological Investigations of an Active Margin* (Ed. by S.F. McGill & T.M. Ross), *Geol. Soc. Am. Cord. Sec. Guidebook*, **27,** 302–318.

G , G.K. (1874) *Progress report*. U.S. Geog. & Geol. Surv. W. 100th Mer.

G , G.K. (1928) Studies of Basin-Range structure. *U.S. Geol. Surv. Prof. Pap. 153*.

G , G.K. (1890) L B . *U.S. Geol. Surv. Mon. 1*.

G , J. & E , M. (1993) 3D-DEF: a user's manual. *U.S. Geol. Surv. Open-File Report 93–547*.

G , J. & E , M. (1994) Topography and tectonics of the central New Madrid seismic zone: results of numerical experiments using a three-dimensional boundary element program. *J. Geophys. Res.*, **99,** 20299–20310.

H , W.K. (1976) Patterns of displacement along the Wasatch fault. *Geology*, **4**.

H , W.B. (1988) Death Valley tectonics; hingeline between active and inactivated parts of a rising and flattening master normal fault. In: *Geology of the Death Valley Region* (Ed. by J.L. Gregory & E.J. Baldwin), pp. 179–205. South Coast Geol. Soc., Santa Ana, CA, United States.

H , W.B. (1989) Crustal geologic processes of the United States. In: *Geophysical Framework of the Continental United States* (Ed. by L.C. Pakiser & W.D. Mooney), *Geol. Soc. Am. Memoir*, **172,** 743–781.

H , G.S., A , R.S. & W , K.X. (1999) Beyond power: bedrock river incision process and form. In: *Rivers Over Rock: Fluvial Processes in Bedrock Channels, Amer. Geophys. Union Geophys. Mono. 107.*

H , T.C., B , R.C., L , K.R. & W , R.E. (1984) Modification of wave-cut and faulting-controlled landforms. *J. Geophys. Res.*, **89,** 5771–5790.

H , D.J. (1997) Landscape evolution at the margin of the Basin and Range. *Geology*, **25,** 1111–1114.

H , D.L., S , D.S. & L , W.P. (1993) The mechanics of continental extension in western North America; implications for the magmatic and structural evolution of the Great Basin. *Earth Planet. Sci. Lett.*, **117,** 59–71.

H , A.M., D , W.E., N , K. & F , R.C. (1997) Soil production and landscape equilibrium: Hillslope analysis using cosmogenic radionuclides in northern California and coastal Oregon. *EOS*, **77,** F245–F246.

H , K.V., M Kenna, L.W., Stock, J., Knapp, J., Page, L., Sternlof, K., Silverberg, D., Wüst, G. & W , J.D. (1989) Evolution of extensional basins and Basin and Range topography west of Death Valley, California. *Tectonics*, **8,** 453–467.

H , D.K., F , R.J. & L , D.R. (1994) The Death Valley turtlebacks reinterpreted as Miocene-Pliocene folds of a major detachment surface. *J. Geol.*, **102,** 718–727.

J , J.A. & W , N.J. (1989) Normal faulting in the upper continental crust: observations from regions of active extension. *J. Struct. Geol.*, **11,** 15–36.

J , C.H., U , J.R. & S , L.J. (1996) The role of gravitational potential energy in active deformation in the southwestern United States, *Nature*, **381,** 37–41.

K , H.M. (1988) Formation of inner gorges. *Catena*, **15,** 433–458.

K , C.R. (1909) Di erential e ects of eolian erosion upon rock belts of varying induration. *Science*, **29,** 753.

K , C.R. (1910) Relations of present profiles and geologic structures in desert ranges. *Geol. Soc. Am. Bull.*, **21,** 543–564.

K , G.C.P. & E , M. (1990) The origin of large local uplift in extensional regions. *Nature*, **348,** 689–693.

K , G.C.P., S , R.S. & R , J.B. (1998) The growth of geologic structures by repeated earthquakes. 1: Conceptual framework. *J. Geophys. Res.,* **93,** 13307–13318.

K , N. & W , R. (1990) Neogene evolution of the Wasatch Fault. *EOS*, **71,** 1584.

L , A.H. & S , J.H. (1978) Models of an extending lithosphere and heat flow in the Basin and Range Province.

In: *Cenozoic Tectonics and Regional Geophysics of the Western Cordillera* (Ed. by R.B. Smith & G.P. Eaton), *Geol. Soc. Am. Mem.*, **152,** 209–250.

M , W.F., D , N.F. & B , T.M. (1978) Landslide occurrence in the Western and Central Northern Rocky Mountain Physiographic Province in Idaho. In: *Forest Soils and Land Use: Proceedings of the Fifth North American Forest Soils Conference* (Ed. by C.T. Youngberg), pp. 116–139. C.S.U., Ft. Collins, CO.

M , C.M. (1990) Soils and geomorphic evolution of bedrock facets on a tectonically active mountain front, western Sangre de Cristo Mountains, New Mexico. *Geomorphology*, **3,** 301–332.

M , D. & E , M.A. (1994) Introduction to special section on tectonics and topography. *J. Geophys. Res.,* **99,** 12135–12141.

M , M.G. (1991) High-angle origin of the currently low-angle Badwater turtleback fault, Death Valley, California. *Geology*, **19,** 372–375.

M , P., B , E.T., B , B.C., D Q , F X , L J , R , G.M., S J , W Z , Y , F. & Y H (1994) Quaternary climate change and the formation of river terraces across growing anticlines on the north flank of the Tien Shan, China. *J. Geol.*, **102,** 583–602.

M , D.R. & D , W.E. (1992) Channel initiation and the problem of landscape scale, *Science*, **255,** 826–830.

R , A., D , W.E., R , R., V , G.K. & R -I , I. (1995) Geomorphological signatures of varying climate. *Nature,* **374,** 632–635

R , N.A. & A , R.S. (1994) Hillslope and channel evolution in a marine terraced landscape, Santa Cruz, California. *J. Geophys. Res.*, **99,** 14013–14029.

S , K.M. & M , D.R. (1995) Limits to relief. *Science*, **270,** 617–620.

S , R.P. (1940) Geomorphology of the Ruby-East Humboldt Range, Nevada. *Geol. Soc. Am. Bull.*, **51,** 337–372.

S , E.E. & A , R.S. (1996) Erosion rates of Laramide summit surfaces: implications for late Cenozoic increases in summit elevations. *Geol. Soc. Am. Abst. Prog.*, **28,** A515.

S , L.J., E , P.C., W , B.P. & C , R.L. (1987) A physical model for Cenozoic extension of western North America. In: *Continental Extensional Tectonics* (Ed. by M.P. Coward, J.F. Dewey, P.L. Hancock), *Geol. Soc. Spec. Publ.*, **28,** 187–201.

S , W.G. (1985) Vegetation and climates of the last 4500 years in the vicinity of the Nevada Test Site, south-central Nevada. *U.S. Geol. Surv. Prof. Pap. 1329.*

S , J.E. (1901) Origin and structure of the Basin Ranges. *Geol. Soc. Am. Bull.*, **12,** 217–270.

S , R.S., K , G.C.P. & R , J.B. (1988) The growth of geologic structures by repeated earthquakes. 2: Field examples of continental dip-slip faults. *J. Geophys. Res.,* **93,** 13319–13331.

S , J.H. (1978) Basin-range structure in western North America; a review, in Cenozoic tectonics and regional geophysics of the Western Cordillera. *Mem. – Geol. Soc. Am.*, **152,** 1–31.

S , J.D. & M , D.R. (1995) Can we predict the rate of bedrock river incision using the stream power law?, *EOS, Transactions*, **76,** F277.

W , R.E. (1978) Geometry and rates of change of fault-generated range fronts, north-central Nevada. *J. Res. U.S. Geol. Surv.*, **6,** 637–649.

W , J.K. & K , G.D. (1989) Flexural uplift of rift flanks. *J. Geophys. Res.*, **94,** 13919–13950.

W , B. (1992) Cenozoic extensional tectonics of the U.S. Cordillera. In: *The Geology of North America* (Ed. by B.C. Burchfiel, P.W. Lipman & M.L. Zoback), v. G-3, pp. 553–581.

W , B.P. & A , G.J. (1988) On the role of isostasy in the evolution of normal fault systems. *Geology*, **16,** 848–851.

W , S., B , C. & F , P. (1993) Mechanical model for the tectonics of doubly vergent compressional orogens. *Geology*, **21,** 371–374.

W , G. (1994) A statistic for testing the elevation characteristics of landscape simulation models. *J. Geophys. Res.,* **99,** 13987–13996.

W , J.A., S , H.E. & F , C.E. (1997) Molnar, Peter, Paleobotanical evidence for high altitudes in Nevada during the Miocene. *Science*, **276,** 1672–1675.

W , L.A., O , J.K. & T , B.W. (1974) Turtleback surfaces of Death Valley viewed as phenomena of extensional tectonics. *Geology*, **2,** 53–54.

APPENDIX: MODEL AND EXPERIMENT DESCRIPTION

Details of the model *Zscape* can be found in Densmore *et al.* (1998), but for the sake of completeness, the essence of the model is described here. Experimental parameter values are given below in Table 1; these are the same as used in Densmore *et al.* (1998) with the exception during some experiments of varying fault geometry, timing of faulting and the use of orographic precipitation.

Zscape is a suite of finite-di erence algorithms based on a uniformly gridded surface that is given an initial random topography of ± 5 m. Erosion and deposition in the model are governed by the conservation of mass so that the rate of change of elevations is given by the spatial gradients of sediment flux,

$$\frac{\partial z}{\partial t} = -\frac{1}{\rho} \nabla \cdot q_s \tag{1}$$

where $\partial z/\partial t$ is the rate of elevation change with time, ρ is the bulk density of the relevant material, and q_s is mass sediment transport rate per unit width. Grid points (nodes) of the landscape are either hillslopes or channel. Hillslopes are characterized by a regolith or soil thickness and a slope. Regolith thickness increases over time and is transported downslope by di usive processes. Regolith production is given by:

$$\frac{\partial R}{\partial t} = \left(\frac{\partial R}{\partial t}\right)^0 + \left[\frac{\left(\frac{\partial R}{\partial t}\right)^* - \left(\frac{\partial R}{\partial t}\right)^0}{\left(\frac{\partial R}{\partial t}\right)^*}\right] R \tag{2}$$

when $0 \leq R \leq R^*$

$$\frac{\partial R}{\partial t} = \left(\frac{\partial R}{\partial t}\right)^* \exp\left[\frac{R^* - R}{R_{\text{scale}}}\right] \tag{3}$$

when $R > R^*$, where R is the regolith thickness $(\partial R/\partial t)_o$ is the bare bedrock regolith production rate, $(\partial R/\partial t)^*$ is the maximum production rate at thickness R^*, and R_{scale} is the exponential decay lengthscale (Densmore *et al.*, 1998).

The transport of reglolith is governed in the model by a linear di usive process:

$$q_s = -k \nabla \cdot z \tag{4}$$

where k is a di usion coe cient. Combining eqns 1 and 2 yields a di usion equation for topography:

$$\partial z/\partial t = \kappa \nabla^2 z. \tag{5}$$

Here $\partial z/\partial t$ is the rate of change of the surface elevation and κ is the topographic di usivity (equivalent to k/ρ).

Fluvial processes of transport and incision are governed by the stream power per unit bed area,

$$\Omega = \gamma A P C_r S/w \tag{6}$$

where γ is the flow unit weight, A is the contributing drainage area, P is the precipitation rate, C_r is the runo coe cient, S is the channel bed slope and w is the flow width. The rate of precipitation rate is 1 m yr^{-1}, and is both spatially and temporally constant in all experiments except for expt 6, which uses an orographic precipitation function. Channel width,

$$w = k_w \cdot \sqrt{A} \tag{7}$$

where k_w is an empirically determined constant (Table 1).

A landscape node becomes a channel node if the stream power is above some critical threshold, Ω_0, which is determined by visual inspection (see Densmore *et al.*, 1998; for details). Sediment bedload transport is governed by stream power in excess of that threshold,

$$Q_s = k_a \cdot (\Omega - \Omega_0) \tag{8}$$

where Q_s is the potential volumetric sediment transport rate per unit bed width, and k_a is an empirical proportionality constant. Any excess stream power, defined as the available power beyond that required to transport all sediment in a particular node, erodes the bedrock channel bed at a rate given by

$$\frac{\partial z_b}{\partial t} = k_b \cdot \Omega_{excess} \tag{9}$$

where k_b is an empirical proportionality constant and Ω_{excess} is the excess stream power. An algorithm for bedrock landsliding is derived from the Culmann slope stability criterion (Spangler & Handy, 1982), which balances the shear strength of a potential failure plane to the maximum stable height of a hillslope, H_c, where

$$H_c = \frac{4C}{\rho g} \frac{\sin \beta \cdot \cos\phi}{[1 - \cos(\beta - \phi)]} \tag{10}$$

and where C is the e ective cohesion on the plane, ϕ is the e ective friction angle on the plane, ρ is rock density, g is gravitational acceleration, and β is surface slope. We define a probability of failure to be

$$p_{fail} = \frac{H}{H_c} \tag{11}$$

that varies between 0 and 1. H is the hillslope height. We take the true failure probability to be the base probability plus a term that increases linearly through time at a rate dictated by the time since the last landslide at that node. This crudely accounts for time-dependent weakening of the failure plane and rock mass. At this stage, however, we neglect the influence of fluids and fluid pressures within the rock mass, which will become important when evaluating the influence of climate change on landscape morphologies. We further assume that bedrock landslides will begin at the toes of unstable slopes, which we base on limited field data (Megahan *et al.*, 1978; Kelsey, 1988) and simple physical experiments (Densmore *et al.*, 1997). Further details of the model landslide behaviour can be found in Densmore *et al.* (1998) and in the body of this paper.